AN OPHTHALMIC ARGON LASER PHOTOCOAGULATION SYSTEM: DESIGN, CONSTRUCTION, AND LABORATORY INVESTIGATIONS

BY *Francis A. L'Esperance, Jr.*, M.D.

THE DEVELOPMENT OF THE LASER IN 1960[1] made available to the world for the first time an extremely bright, monochromatic, highly directional beam that operated in the visible portion of the spectrum. It quickly became apparent to ophthalmic investigators[2–4] that the potential use of the laser principle in photocoagulation was enormous. The increased predictability of the absorption of laser radiation by the ocular structures, the precise focusing capabilities of the monochromatic, coherent beam, and the high photon-energy density were attractive facets of the laser principle. The first actual laser photocoagulation trials in 1961[2] and 1963[3] supported these contentions and, in addition, showed that pulsed ruby laser photocoagulation was efficient, highly effective, and required no anesthesia or akinesia.

Ruby laser photocoagulation has been successfully used in the treatment of many ocular diseases, but it has been demonstrated to be grossly ineffective for most varieties of ophthalmic vascular disease.[5–7] Areas of neovascularization, telangiectatic or aberrant vessels, and angiomata are highly refractory to ruby laser radiation, although microaneurysms can be obliterated in a small percentage of the cases.[5] With the ruby laser, the distinctly advantageous features of laser irradiation are not effectively utilized in the treatment of vascular abnormalities, since the red output beam is not appreciably absorbed by blood vessels or hemoglobin. Therefore, vascular disease of the eye —the second leading cause of blindness in this country—had, until recently, no other treatment available except photocoagulation by the non-specific broad coagulations of the xenon-arc source or therapy by extraocular methods.

The recent discovery of the argon, krypton, and xenon ion lasers has provided the scientific community with laser emission lines in every

TR. AM. OPHTH. SOC., vol. 66, 1968

portion of the visible spectrum. It became possible, therefore, to select laser wavelengths that would be absorbed by hemoglobin. The argon laser (4579 Å–5145 Å) produces radiation at eight to ten wavelengths in the blue-green spectral region, two wavelengths (4880 Å and 5145 Å) comprising relatively powerful emissions. A gross comparison of the argon emission range with known hemoglobin absorption curves shows that sufficient energy can be absorbed by blood vessels to cause intravascular coagulation. This observation and the relative ease with which the inert argon gas can be made to "lase"—as compared with krypton and xenon—were the deciding factors in selecting the argon laser as the basis for the development of a photocoagulation system that would be effective in the treatment of ophthalmic vascular disease.

DEVELOPMENT OF AN OPHTHALMIC ARGON LASER PHOTOCOAGULATION SYSTEM

High Power Argon Laser for Ophthalmic Use

When the project to develop an argon laser for the treatment of ophthalmic vascular disease was conceived, we had little idea of the power levels necessary for the successful coagulation of ocular tissue, nor did we have any conception of the optical losses that would be encountered in the delivery system. We therefore arbitrarily decided to construct an argon laser with an output power in the two- to five-watt range. During the initial development of the power supply for the argon laser, we realized that it might be possible to achieve powers between five and ten watts with the proper instrumentation. These power levels would allow us to perform tissue studies involving the effect of high-photon-density bombardments.

The Raytheon Corporation of Waltham, Massachusetts, undertook the formidable task of constructing a laser of this output power at its Special Microwave Devices Laboratory. Significant problems arose during the development phase, but the powers requested were produced by employing several optical techniques.

The first technique was the utilization of large-bore discharge tubes in place of the commonly used 1- to 3-mm size. The term "large bore" designates a 4- to 8-mm diameter as a representative range. The processes involved in a double-diameter laser site centered around the operating current that must be used, since the doubling of the conventional bore size would lead to a fourfold increase in the operating

current to maintain the current density. It was found that the voltage gradient could be cut approximately in half, necessitating only a doubling of the input power. Since the cooling perimeter also doubled, the wall thermal loading was unchanged. The optical gain remained reduced, but since it is already reasonably high in argon ion lasers, a downward readjustment of the output mirror transmissivity brought about a new optimum coupling. Thus, as long as the gain remained significantly above the unavoidable resistive optical losses, this readjustment would be quite effective.

The application of an optimized axially-directed magnetic field also was differentially favorable in output power to the double-size tube. The field-favorable factor was approximately two, yielding a total output power gain of six or seven over the original laser design. Since the latter had a rating of 1.5 to 2 watts for a 3-mm bore, we had escalated the power of the new laser to the 10-watt level—the most powerful argon ion laser in existence.

MODEL LG-13S ARGON ION LASER

Raytheon's Model LG-13S argon ion laser, shown in Figure 1, is an extremely high-power, low-divergence light source, designed specifically for our use, capable of producing continuous output in either a multimode or single transverse mode pattern in nine wavelengths between 4579 Å and 5145 Å (the blue-green portion of the visible electromagnetic spectrum). The LG-13S laser system incorporates laser head Model LG-13S and laser power supply Model LP-46S. This laser system is designed to produce a total power output of 10 watts continuous wave (cw) in the diffraction-limited, single transverse (TEM_{00}) mode distributed over the nine available wavelengths. At the 10-watt level, the principal wavelengths are 4880 Å, 5145 Å, and 4765 Å, and their output powers are 4.00, 2.50, and 1.25 watts, respectively, when the standard resonator mirrors peaked at 5000 Å are used. The output power levels for each particular wavelength may be increased slightly with optional resonator mirrors peaked at that wavelength.

The laser cavity is approximately 90 inches long, which allows about 5 inches between the tube end and one mirror for intracavity experimentation. Sufficient area has been left on the laser base to mount a dispersion prism for wavelength selection internal to the laser, if desired.

The laser tube has a 60-inch-long main discharge capillary with an

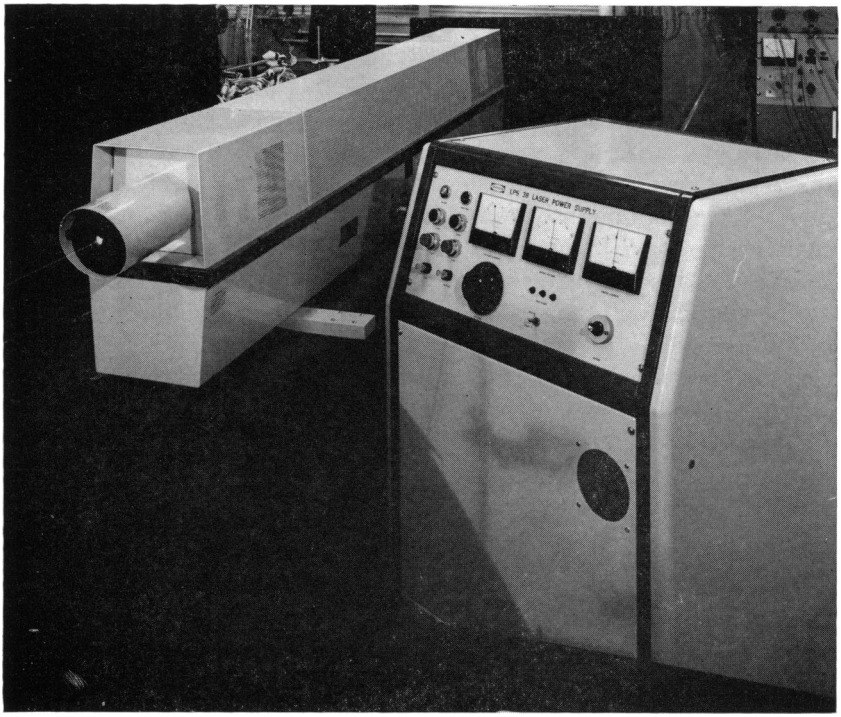

FIGURE 1
Photograph of the 10-watt Raytheon Model LG-13S argon ion laser, designed and constructed specifically for ophthalmic investigation.

inside diameter of 4.0 mm. The capillary tube is cooled by water flowing through the annular jacket. The laser tube is supported by adjustable mounts at both ends and at the center, as well as at each of the electrode bulbs, to allow precision tube alignment and to provide protection against mechanical shock.

The Model LG-13S 10-watt argon laser head specifications, in addition to those mentioned, include an output power ripple less than 1 per cent peak to peak and a wavefront that is diffraction-limited, uniphasic, coherent, and spherical, operating in a single transverse mode for each wavelength. The beam diameter varies with the output power and measures 4.0 mm at the exit aperture at full power and 2.5 mm at half power. The beam divergence is less than one milliradian without a collimating telescope, and it is 35 seconds of arc with the telescope. The physical dimensions of the laser head are: length 110 inches, width 18 inches, height 18 inches, and weight 550 pounds.

MODEL LPS-46 POWER SUPPLY

The model LPS-46 power supply used with the Model LG-13S laser system is capable of providing 840 VDC at 30 amperes for the discharge tube and solenoid magnet windings, and 60 VAC at 0 to 60 amperes for the cathode heater supply. The Model LPS-46 laser power supply requires an input power of 480 V, 60 cps, 3-phase at 50 Å The power supply is 48 inches high, 24 inches wide, and 20 inches deep, and weighs 450 pounds.

Intraocular Argon Laser Photocoagulation Delivery System

An extremely intricate and precise optical relay system was constructed in collaboration with the American Optical Special Products Division in Buffalo, New York. The existing target, focusing, and illumination optics of the American Optical ruby laser photocoagulator were retained,[8] but the remainder of the delivery system apparatus was redesigned to be used specifically with the CW argon laser. The components of the intraocular argon laser photocoagulator are illustrated in Figure 2.

Initially, a gimbaled mount intercepts the laser beam, and redirects it horizontally at 90° through two rotating highly reflective dichroic mirrors mounted in ball-bearing sockets. The entire mount swings around pivot points aligned along the axis of the laser beam. Therefore, the reflected beam can be directed along any position in the X and Y axes at right angles to the original beam. A 1.5:1.0 expanding Galilean telescope has been inserted into the first stage of the gimbaled mount. Two pressure bolts can be turned to move the telescope slightly, thereby creating a small motion of the expanded laser beam in the same direction. This addition aids immeasurably in aligning the beam when necessary.

A concentric telescoping steel tube encloses the beam from the gimbaled table mount to the optical head. This four-foot tube can be reduced in length by 16 inches and therefore has an 8-inch inward and outward movement from its midposition. Motion of the optical head is permitted along the Z axis with this interconnecting gimbal-to-optical head tube, as well as along the X and Y axes previously mentioned. The tube links the motion of the gimbaled mount to the laser optical head so that no realignment of the beam is necessary. The laboratory personnel are also protected by enclosure of the beam in the extension tube.

The optical head is supported by a spring-balanced stand mounted on casters. The entire weight of the optical head and extension tube is counterbalanced accurately so that the head may be moved through its full 12-inch vertical excursion by slight pressure. A Y-shaped arm extends from the movable stand and supports the optical head. This

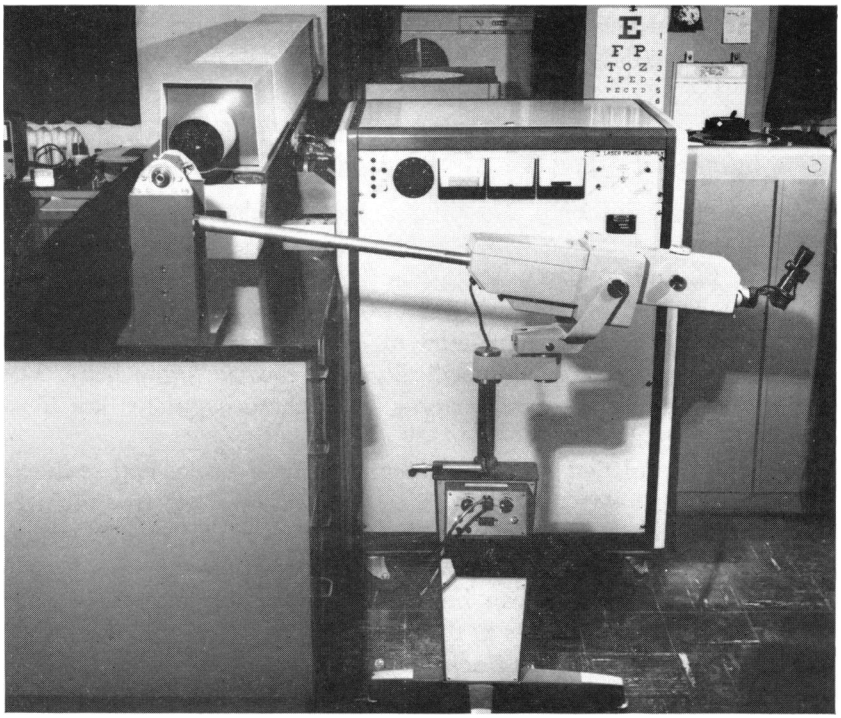

FIGURE 2

Photograph of the intraocular argon laser photocoagulation delivery system, showing the laser, gimbaled table mount, extension tube, support stand, and optical head.

arm has a roller-bearing cradle upon which the head can be moved toward or away from the gimbaled mount, providing 2 inches of movement in that direction. The arm (and head) can be rotated about the axis of the support stand, permitting 10 inches of horizontal movement. In addition to these excursions, necessary for fine adjustment, the entire optical head, support stand, and extension-coupling tube can be moved grossly around the stationary gimbaled mount through an arc of 40° horizontally (30 inches) and 20° vertically (15 inches).

The support stand also houses all electrical equipment including rheostats for the aiming and viewing lights.

The most intriguing portion of the entire intraocular delivery system project was the construction of an optical relay head that would retain the highly advantageous properties of the argon laser beam, yet provide the various optical elements that would make argon laser irradiation a safe and sophisticated method of photocoagulation. The following components were considered essential for the optical head of an intraocular argon laser photocoagulation delivery system (Figure 3):

1. A target system to allow the surgeon to locate the exact intended argon laser impact area before firing
2. Background retinal illumination to visualize the tissues surrounding the impact target area for orientation and evaluation
3. Argon-beam focusing potential to permit the minimal amount of energy necessary for retinal coagulation to be transmitted through the ocular media
4. A viewing system that would have mobility and versatility, provide a large field of view, and neutralize the patient's refractive error
5. Special laser optics, incorporating dichroic mirrors, diffusing elements, and various safety devices particularly effective with argon laser systems.

TARGET SYSTEM

The ability to determine the exact location of the intended coagulation spot before transmitting the laser beam through the eye is the most important feature of any photocoagulation system. A separate target system that directed the target beam coaxially along the same optical path as the laser was used. Any maladjustment of the focusing lenses, obstructions to passage of the laser beam such as the iris border, or impediments along the path of the beam (vitreous debris, pigment accumulations) can be detected before the actual delivery of the light energy. An attenuated argon laser beam was considered, at first, as a possible target indicator, but this proposal was discarded because of the poor beam contrast with the fundus and the inherent laser pulsing difficulties that would be encountered. A separate, coaxial, focusable aiming system that directed a bright, sharply demarcated spot on the area to be photocoagulated was chosen.

The ability to select various coagulation sizes is of considerable clinical significance. Large-sized coagulations are advantageous when a large area is to be treated, when delimiting certain peripheral

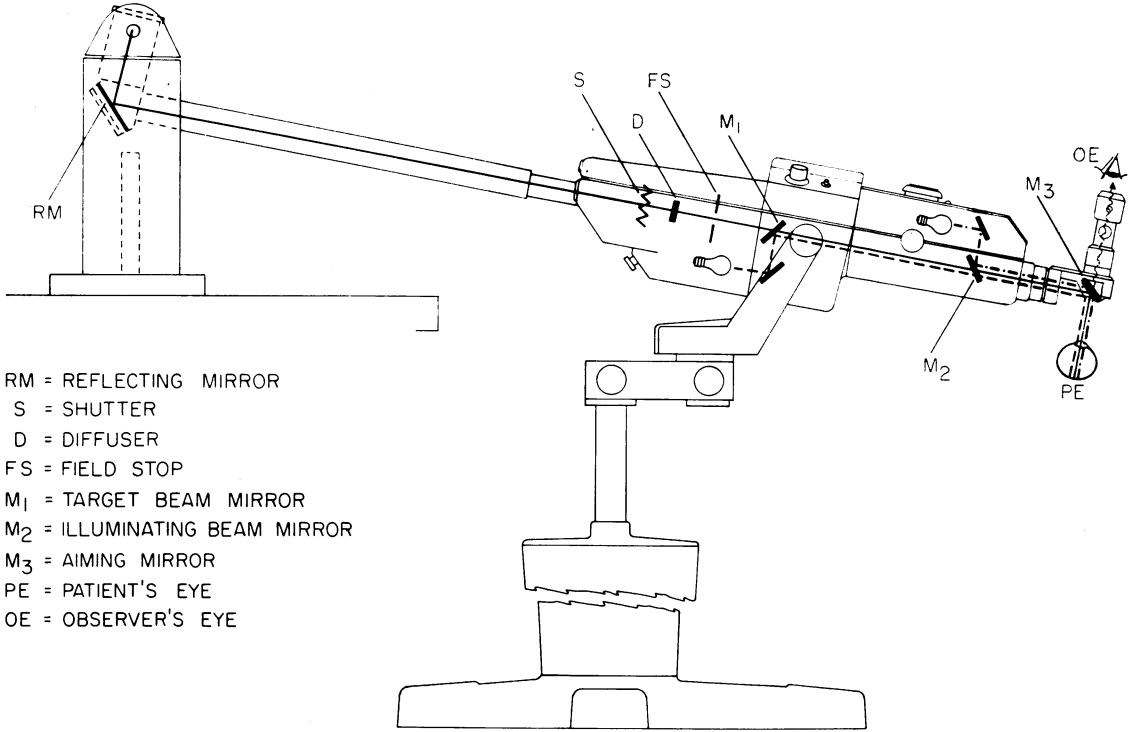

FIGURE 3

A schematic representation of the optical components and beam paths that exist in the intraocular argon laser photocoagulator.

degenerations or retinal breaks, or when a large vascular lesion or arboretum of vessels is to be irradiated. Small coagulations are preferable for posterior retinal work to preserve functional visual area, for areas near the macula or optic disc, and for isolated vascular abnormalities. Furthermore, less energy per square centimeter of irradiated retinal tissues is necessary for large coagulations than for small ones, and the total amount of radiation ultimately entering the eye may be an important factor in some cases. Treating these particular patients with larger-sized coagulations may be beneficial in order to minimize the total energy transmitted through the ocular media.

The aiming spot size projected from the argon laser optical head onto the retina was designed to correspond to the impact diameter of the laser beam. The size of the aiming circle on the retina can be varied to indicate diameters of 1°, 2.5°, and 5°. The aiming beam and laser beam pass through a common field stop so that a change in the field stop size in order to change burn size will change both the aiming spot and laser beam size correspondingly. The common field stop also functions to insure that the laser beam is coupled optically to the aiming spot, and that both beams will be focused exactly at the same ocular plane.

BACKGROUND RETINAL ILLUMINATION

An illuminated circular viewing area, measuring about 20° in diameter, surrounds the aiming spot. This illumination is obtained by imaging the filament of the tungsten lamp on the patient's pupil like the illumination beam in indirect ophthalmoscopy. The intensities of the aiming and viewing beams are variable and are controlled by separate rheostats. Usually the weakest background illumination beam intensity consistent with the clarity of the ocular media is used, in order to provide a highly contrasted aiming spot.

Dichroic mirror M_2 is designed to reflect approximately 60 per cent of the white light from the tungsten lamp except for the region of the transmitted argon wavelengths. Dichroic mirror M_3 reflects between 40 and 60 per cent of the white light impinging upon it, depending on the angle of incidence of the light, so that about 1/4 of the light produced by the lamp actually reaches the patient's eye. The surgeon sees only 40 to 60 per cent of the light emerging from the eye minus the argon band, and therefore can appreciate only 1/16 to 1/8 of the original amount of light. Nevertheless, the background retinal illumination is excellent and entirely adequate for photocoagulation purposes.

FOCUSING POTENTIAL

The patient's refractive error must be optically corrected in order to produce small coagulations of proper intensity. The size of the treated spot cannot be accurately predicted without neutralization of the refractive error. For the highly ametropic eye, it might be extremely difficult to create a retinal coagulation without reverting to higher energy transmission across the ocular media. In addition, treatments in the periphery or on highly elevated tumors or intravitreal vessels would be very difficult unless the beam could be focused.

The design utilized in the optical head of the argon laser provides a substantial correction range without excessive motion of lenses. An afocal telescopic system with a magnification of three gives a correction range of −12 to +18 diopters with a motion of 24 mm. The system has the property of constant magnification regardless of object dis-

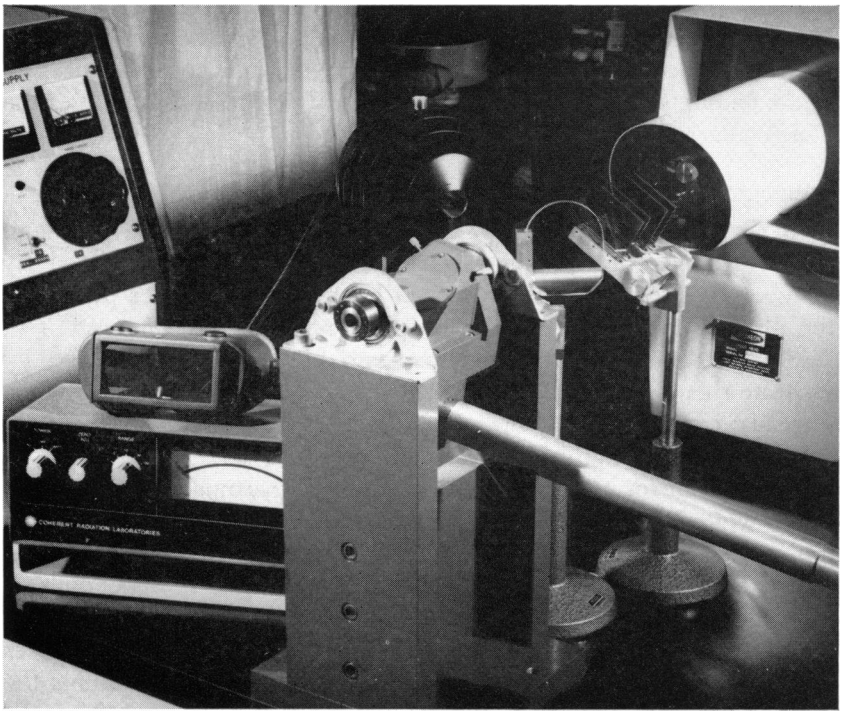

FIGURE 4

Photograph of special laser optical devices utilized during photocoagulation procedures: antiargon goggles, power meter, beam splitter and attenuation filters near gimbaled mount, and extension tube.

tance. Therefore, the size of the target spot, the angular size of the beam going into the patient's eye, and the position of the eye will not change with adjustments of the lenses.

An intense aiming spot of white light passes through the same optical mechanism as the laser beam and, when focused on the patient's fundus, will indicate the exact size and coagulation position of the laser beam. In this manner, the laser beam can be brought to a precise focus on any visible portion of the ocular structures by the preliminary adjustment of the target spot. By moving the afocal telescopic lens system, a clear, sharply defined circular spot can be obtained. Intravitreal blood vessels, iris abnormalities, lid lesions as well as chorioretinal defects can be treated with the minimum amount of energy necessary for coagulation. This facet of the system becomes extremely important when periods longer than one second per pulse are required for adequate treatment.

VIEWING SYSTEM

A focusable, 1/3 power telescope with a 20° field of view and five times effective magnification in viewing the fundus of an emmetropic eye was employed in this instrument. The hand-held telescope is connected to the dichroic mirror, M_3, by a 2 : 1 angular reduction linkage. The fundus lesion is viewed through the telescope, and the aiming spot is focused upon the area. The firing button is located on the telescope mount, so that it may be easily depressed for firing. This button actuates a microswitch that opens a shutter while the button is depressed. The argon beam passes through the shutter into the optical system to be eventually deflected by the mirror, M_3, into the patient's eye.

The 1/3 power telescope is conveniently maneuverable and is capable of viewing an 80° arc in an axis parallel with the optical head and 160° perpendicular to it. Inherent reflective deficiencies in the M_3 dichroic mirror at extreme angles restrict adequate laser treatment in these regions. Visual inspection of the ocular fundus, however, is unimpaired throughout this cone of movement. The telescope can be focused on any portion of the intraocular structures by rotating its head. In this manner, the refractive error of the patient can be optically neutralized within a substantial correction range of -12 to $+18$ diopters. The color balance of the fundus image is excellent, although a slight shift toward the red portion of the spectrum is evident due to elimination and reflection of the blue-green rays from the eye by the M_3 dichroic mirror.

SPECIAL LASER OPTICS

Dichroic Mirrors

The effectiveness of the multilayer mirrors M_1, M_2, and M_3 greatly influences the performance of the instrument. The idealized transmittance curves shown in Figure 5 display the desired characteristics of each mirror, while the actual measured transmittance curves for the

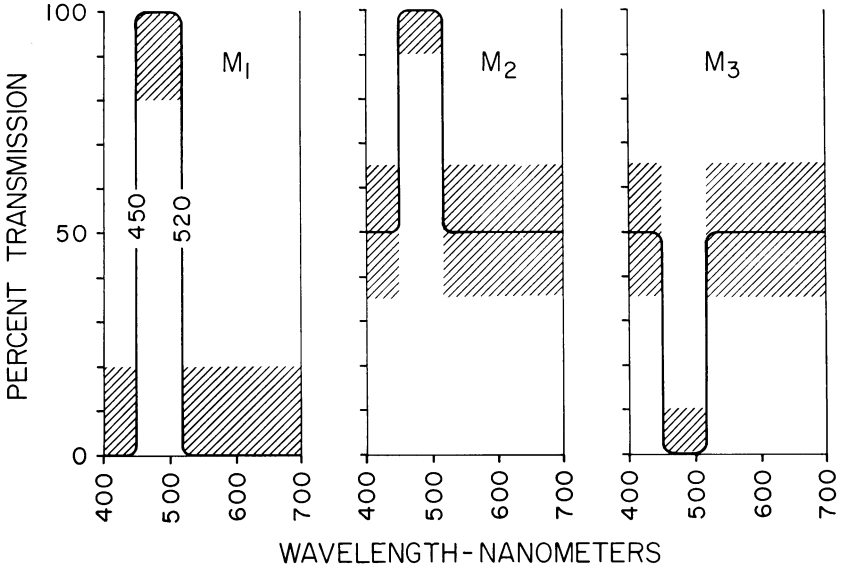

FIGURE 5

The idealized transmittance curves of the three dichroic mirrors—M_1, M_2, M_3—incorporated in the optical head of the argon laser intraocular photocoagulator.

multilayer mirrors vary somewhat from the ideal. Preservation of the color balance of the observed retinal image was attempted by retaining as much visible light as possible outside the argon band in the aiming and viewing beams. Mirror M_1 must transmit all of the argon laser wavelengths (4545 Å–5287 Å), especially the principal wavelengths at 4880 Å and 5145 Å, and reflect the rest of the visible spectrum, i.e., the target beam. Mirror M_2 must transmit the argon laser beam, and reflect 50 per cent of the illuminating beam. Mirror M_3 must reflect the argon laser wavelengths entirely and transmit 50 per cent of the remainder of the spectrum at all angles between 15 and 55° of beam incidence, i.e., reflect 50 per cent of the target and illuminating beam into the patient's eye and transmit 50 per cent of the light

from the fundus into the observer's eye. The scattering factor of mirror M_3 was kept much below 0.5 per cent since the scattering potentials of visible light, and especially the argon beam, could markedly decrease the contrast of the fundus image.

Diffusers

The beam spread of a typical argon laser assumes a Gaussian-shaped distribution with gradual falloff of energy with increasing angle from the axis. The retinal impact of a low-energy laser beam might create a coagulation smaller than a higher energy beam, because only the peak of the beam's energy is used in the former case. Also, higher energy radiation will heat the tissue surrounding the target spot by thermal conduction, and the greater the energy in the spot, the larger will be the affected area.

These situations lead to a heat distribution which is highly concentrated at the center of the lesion relative to the edge. In order to provide a more uniform energy distribution with lesion diameters up to 5°, to concentrate the laser energy at the retina rather than the pupillary plane, and to avoid the concentration of energy near a mirror or lens in the optical system, it was necessary to insert a diffuser between the laser beam and the first telescope lens. The diffuser destroys some of the collimation as well as the spatial coherence of the beam, but does produce a fairly uniform energy intensity across the burn diameter. The various burn sizes can be produced by interposing the appropriate diffuser and its associated field stop on the optical axis at a position conjugate to the patient's pupil. Since the argon laser beam is 4 mm in diameter at the diffuser, the 0.7 magnification of the optical system reduces the laser beam diameter at the patient's pupil to about 3 mm. This diameter is small enough to pass easily through a dilated pupil and large enough to give a low energy density at the pupillary plane.

PHOTOCOAGULATION PROCEDURE

The patient is treated in the reclining position with the optical head positioned in the approximate meridian of the intraocular lesion. The background viewing light is directed through the dilated pupil and the appropriate target beam is selected and focused. The laser power is attenuated to a low level and gradually raised until the proper coagulation reaction is observed. The remainder of the photocoagulation procedure is performed in the manner that has become routine with other continuous sources such as the xenon-arc lamp.

Biomicroscopic Delivery System for Anterior Segment Photocoagulation

The utilization of a biomicroscope as a delivery system to transport a laser beam from its source to the eye has several distinct advantages.

1. The target area can be viewed binocularly and stereoscopically.
2. The target tissue can be viewed with varying powers of magnification.
3. Precorneal and contact lenses can be used with the biomicroscope for visualization of the fundus or anterior chamber angle.
4. A moderate degree of mobility is available with the biomicroscope than enables photocoagulation to be performed with some versatility.
5. Photographic systems can be adapted to some biomicroscopes (Zeiss) that allow concurrent recordings of photocoagulation procedures.
6. The biomicroscope has distinct advantages over any other existing observation system for anterior segment photocoagulation and certain animal threshold studies.

The biomicroscope delivery system was fabricated and assembled at the Bell Telephone Laboratories in Murray Hill, New Jersey, under the supervision of Edward F. Labuda, PH.D. The basic design of the beam-splitter type of slit-lamp biomicroscope manufactured by Carl Zeiss, Inc., of Oberkochen, West Germany, was modified to accommodate the argon laser beam without appreciable power losses at the optical components and with maximum safety for the surgeon. The unmodified beam-splitter mount is constructed with two viewing or photographic systems available in addition to the surgeon's observation system. This beam splitter "splits" the rays of light from the patient's eye into two portions—one portion entering the surgeon's eyes at the eyepieces and the other portion entering the secondary observation tube or camera. Our fundamental conceptual shift of design was to coat one of the beam-splitter cubes so that it would deflect the laser beam into the patient's eye for photocoagulation, while retaining the other beam-splitter cube for photographic purposes. In addition, the observation system for the surgeon was altered slightly so that the view of the target area continued to be sharp and bright despite the elimination of the argon spectrum.

The Zeiss beam-splitter accessory was dismantled and the entirely new beam-splitter cubes were introduced (Figure 6). One of these cubes was specifically coated on sides 4, 5, and 6 with an antireflection

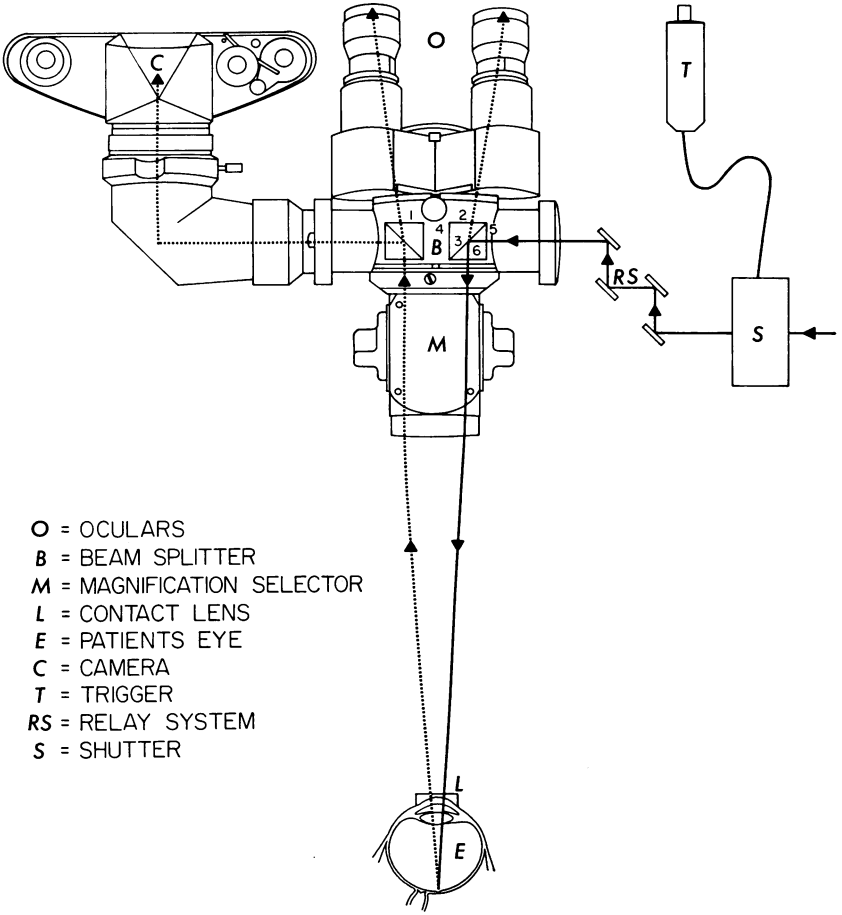

FIGURE 6

Diagram of the biomicroscopic delivery system for anterior segment (and selected paramacular) photocoagulation with argon laser radiation. The beam passes through a triggered shutter and relay system to the beam-splitter cube. The dichroic diagonal face of the cube reflects the argon beam through the magnification selector to the patient's eye. Simultaneous visualization and photography are performed through protective antiargon filters.

coating. The intracube diagonal splitter face, 3, was coated with a dichroic film that reflected all of the argon wavelengths and allowed high transmission of the rest of the visible spectrum. The faces of the cubes nearest to the observer, sides 1 and 2, were covered with an anti-argon spectral film to prevent the entrance of any stray argon energy into the observer's eye.

The argon beam is introduced into the beam splitter from the laser or intermediate articulated-arm delivery system (with adapter) and is deflected away from the observer through the telescopic magnification selector toward the objective lens of the slit-lamp, as shown in Figures 6 and 7. The objective lens (100–200 mm focal length) then focuses the beam on the target tissue. This tissue can be located externally in the anterior segment in the region of the trabeculum or in the fundus of the eye. The latter two ocular areas require the ancillary use of a contact lens (Thorpe, Goldmann, or Worst lenses) or a precorneal lens (Hruby, Rubin) to achieve the proper focus. The addition of a −1- or −2-diopter lens before the delivery system inlet, or the movement of the oculars away from proper adjustment will create a disparity between the focus of the observation system and the argon photocoagulation system. This maneuver will permit a larger coagulation spot to be produced by the unfocused beam when this is desired.

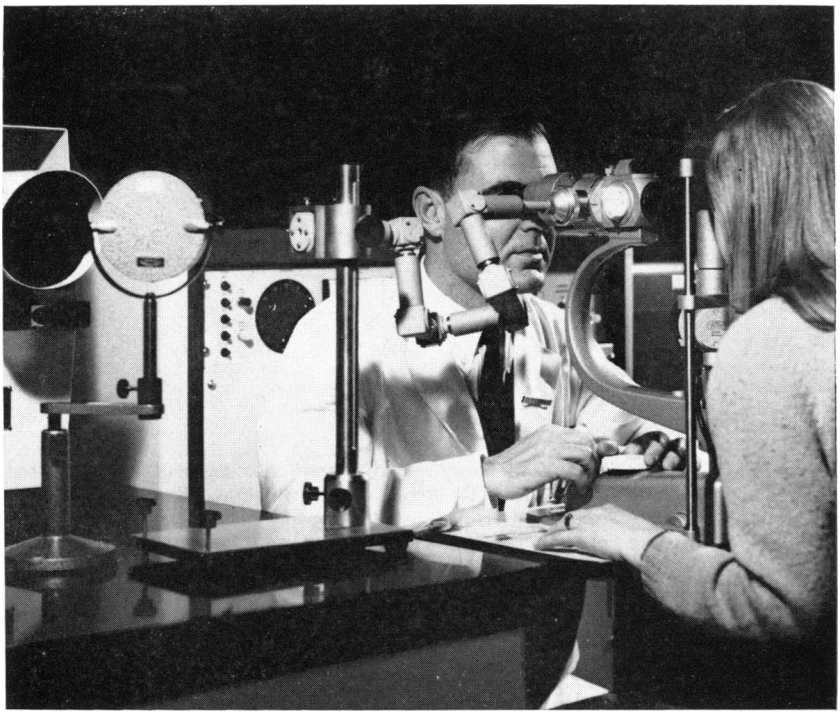

FIGURE 7

Photograph of the biomicroscopic delivery system during argon laser photocoagulation showing the articulated-arm relay system, adapter, and slit lamp in an operational attitude.

Generally, the biomicroscope is utilized because of its ability to cauterize minute areas, and the purposeful defocusing of the argon beam is not usually employed.

The focusing precision of the beam can be enhanced even further by the use of the higher power telescopic couplets in the magnification portion of the microscope (25×, 40×). The higher the magnification, the more shallow will be the depth of focus and therefore the depth of coagulation. By employing higher power couplets in this manner, extremely discrete coagulations on the order of 0.001 mm^3 can be produced.

Prior to actual photocoagulation, a highly attenuated argon beam is transmitted through the instrument and directed upon the target. Since the visualization and photocoagulation optical systems are the same, the beam can be brought to a sharp focus by simply manipulating the slit lamp until the target tissue is clearly seen. A foot or hand trigger is then pressed that electrically removes the attenuating neutral density filter from the path of the beam. The full predetermined power of the argon beam then travels through the delivery system to the coagulation site. The length of each burst of light can be regulated by a precise shutter mechanism or can be controlled manually to create the desired photocoagulation effect. Although the observer's eyes are protected from the argon radiation, all aspects of the photocoagulation process can be observed without difficulty. Simultaneous cinematography during the coagulations has been a valuable documentary procedure.

Articulated-Arm Delivery System for Surface Photocoagulation

The need to construct a system that would transmit the laser beam through a flexible, easily movable mount has been apparent for several years. A new device has been developed that guides the beam from the laser source through hollow, jointed arms to a small handle. The handle is approximately the size of a fountain pen and can be moved easily in any direction by the surgeon. The handle can be attached to a surgical biomicroscope for anterior segment work. In this case, the beam is transmitted through the jointed arms of the delivery device, introduced into the optical system of the microscope, and directed upon the target tissue by the biomicroscopist.

The system consists of an alternating series of six hollow tubular sections and six hollow blocks, as diagramed in Figure 8. The tubes are connected to the blocks at right angles to each other so that they form an elbow. Prisms within the blocks reflect the laser beam around

each 90° corner. The tubular sections are constructed of inner and outer magesium tubes. One tube is connected to the block on one end and the other tube to the block at the opposite end. Ball bearings set between inner and outer tubes allow free rotation about a common axis. The net result is that the arm, which resembles a series of "L s" strung together, has full tridimensional mobility.

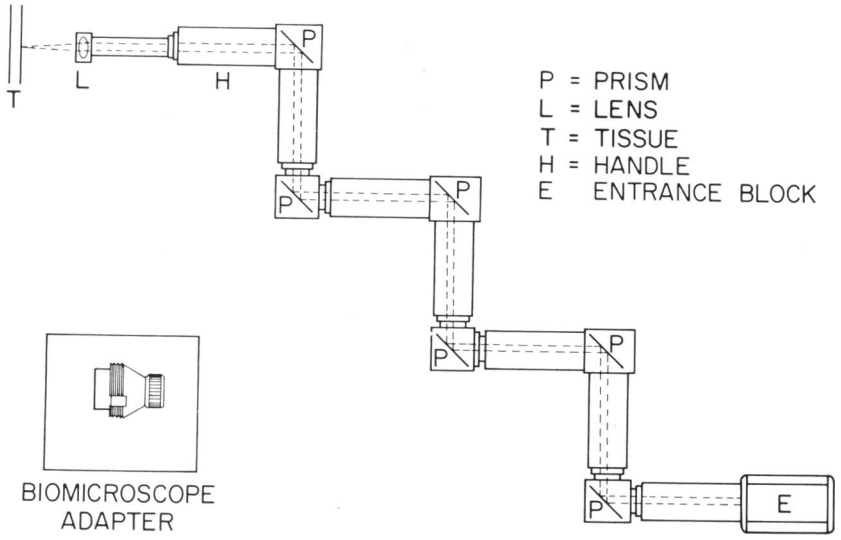

FIGURE 8

Diagram of the articulated-arm delivery system for surface photocoagulation with argon radiation. The beam is reflected by the prisms and focused on the tissue by the convex lens in the handle. The lens may be removed and replaced by an adapter for use as a relay system with the biomicroscope.

Because the tubes swivel and the corners remain rigid, the light always makes 90° turns. After it has been reflected through the tubes, the light exits through the small pen-like handle. The coherence of the laser beam is preserved by the high quality reflective characteristics of the prisms. Thus, with the coherence maintained, the light can be focused to an exceedingly small spot by the photocoagulation instrument. The handle of the articulated arm can be attached with the proper adapter to any of the photocoagulation devices—the optical portion of the intraocular photocoagulator, the biomicroscope, or a modified direct ophthalmoscope head. By incorporating the articu-

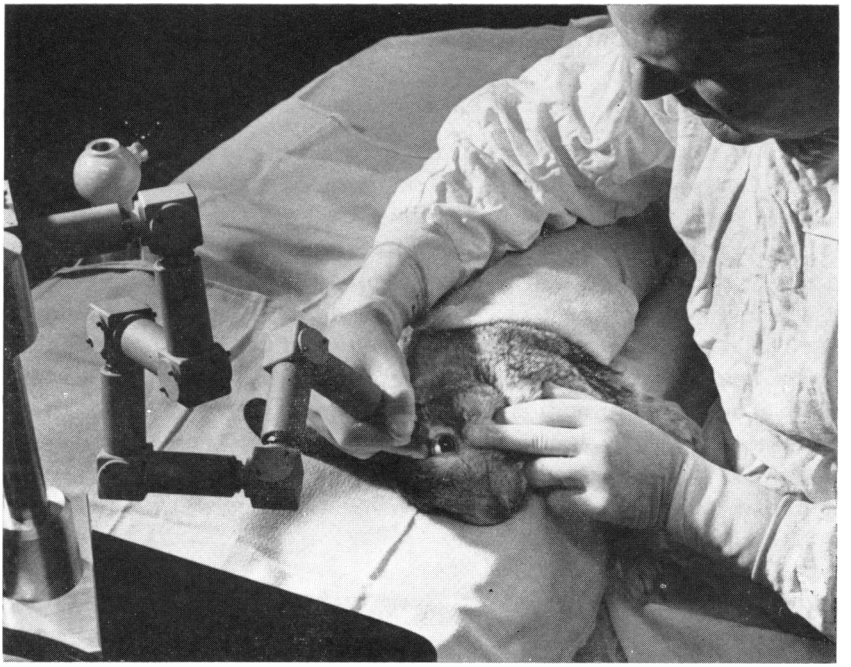

FIGURE 9
Photograph of the articulated-arm delivery system being used as a "light knife" or "photon scalpel" for the photocoagulation and incision of surface tissues.

lated arm as an intermediate delivery system, each of these photocoagulation devices is capable of extreme maneuverability and flexibility (Figure 7). Critical adjustments, observation, and focusing through these instruments are performed much more precisely, more rapidly, and with greater ease.

The addition of a 40-diopter lens to the tip of the handle focuses the light to a point-sized image 25 mm away. With this arrangement, the articulated arm is converted into a highly effective "light knife" that can incise any animal tissue, as shown in Figure 9. Animal testing has demonstrated that complete surgical procedures can be done without the loss of blood. The cutting ability and remarkable hemostatic qualities of the articulated photon scalpel will be discussed more fully in a later report. The articulated-arm system can be used, with the proper modifications, with both pulsed and continuous wave lasers of any visible wavelength, and is the most versatile of the delivery systems developed.

LABORATORY INVESTIGATIONS WITH THE ARGON LASER

In Vitro Studies

Studies were performed that were designed to delineate the *in vitro* effect of argon radiation on various components of the ocular structure. Certain portions of the eye, such as the blood column, were impossible to study quantitatively by histologic techniques. Because these tissues occupy important areas in the region of proposed photocoagulations, it was imperative that the changes occurring with irradiation be documented thoroughly at various power levels. Considering the high absorption of the blue-green wavelengths of argon by hemoglobin and the paucity of information available about the tissue effects from high-intensity monochromatic sources, several diverse studies were conducted that served to demonstrate the hemodynamic effect of argon radiation. A complete report of these investigations will be described in a subsequent communication.[37]

THE VISIBLE SPECTROPHOTOMETRIC PROPERTIES OF A 100-MICRON FILM OF OXYGENATED BLOOD

A thin film of oxygenated blood, close to the thickness of the larger retinal vessels, absorbs more incident radiation (86 per cent) at the argon-ion laser wavelength of 4579 Å than at any other existing laser emission (Figure 10). However, the average argon energy absorption level by hemoglobin ranges between 72 and 74 per cent for a 100-micron film, since the principal wavelengths of 5145 Å and 4880 Å occupy over 90 per cent of the available argon radiation while the 4579 Å emission is relegated to less than 2 per cent of the total argon laser output.

The krypton ion laser wavelengths of 5682 Å and 5308 Å are highly absorbed by hemoglobin with an average absorption (82–84 per cent) that is 10 per cent higher than the average argon absorption for a 100-micron film of oxygenated blood. Power limitations and technical difficulties associated with krypton lasers have hampered investigations into this potentially fertile area for vascular photocoagulation.

Absorption by oxygenated blood at the ruby (6943 Å), longest krypton (6471 Å), and the helium-neon (6328 Å) wavelengths are considered too low for effective use in vascular photocoagulation. On the other hand, high transmission of these particular wavelengths by blood suggests that these emissions may be valuable when attempting

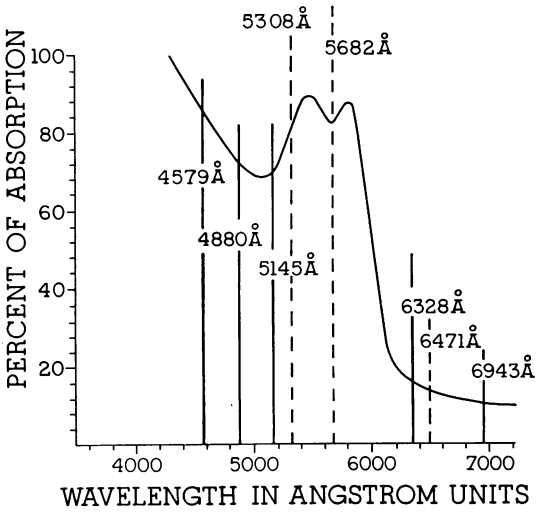

FIGURE 10

The spectrophotometric properties of a 100-micron film of oxygenated blood, showing the high absorption potential for argon and krypton laser radiation, and low absorption potention for helium-neon and ruby laser light.

to preserve vascular function or when attempting photocoagulation through a mild intravitreal hemorrhage.

THE EFFECT OF ARGON LASER RADIATION ON THE BLOOD CONSTITUENTS

Below the substantial energy dose level of 256 watt-seconds per cubic centimeter, there is no appreciable effect of argon radiation, reflected by present chemical assay methods, on any of the particular blood constituents that were investigated. These constituents included cholesterol, calcium, inorganic phosphorous, total bilirubin, albumin, total protein, uric acid, blood urea nitrogen, true glucose, lactic dehydrogenase, alkaline phosphatase, and serum glutamic-oxalacetic transaminase.

THE EFFECT OF ARGON LASER RADIATION ON THE PLASMA PROTEINS

All protein constituents including the albumin, and gamma-I and gamma-II, beta, alpha-II, and alpha-I globulins, and total protein content were within normal limits and did not vary with the time or the power level of the argon irradiation. There appears to be no selective absorption of argon energy or adverse protein change in the plasma

proteins, and they can be considered to be unaffected by argon radiation.

THE COMPARATIVE EFFECT OF ARGON LASER AND XENON-ARC RADIATION ON BLOOD AGAR

The power density required for a threshold lesion on a blood agar plate with the xenon-arc beam was 4.5 times greater than that required for a comparable visible threshold lesion with the argon laser beam. Therefore, histologic effects that depend upon the absorption of incident radiation by hemoglobin can be produced by argon irradiation with 22 per cent of the energy required by the xenon-arc beam for a similar result.

THE COMPARABLE EFFECT OF ARGON LASER RADIATION ON FLUORESCEIN AGAR AND FLUORESCEIN BLOOD AGAR

Studies utilizing a clear solution of agar with varying concentrations of an absorptive dye or absorbent material such as hemoglobin can be used effectively to determine the relative absorption potential of these substances for some given type of visible radiation. A coagulation effect by an unfocused argon laser beam was noted at fluorescein concentration of 0.01 per cent in plain agar with a flux of 0.80 watt-seconds. This particular fluorescein concentration is equivalent to the concentration that would be achieved in a normal individual with a five-liter blood volume, if 10 cc of a 5 per cent sodium fluorescein solution were injected intravenously. These observations would indicate that fluorescein circulating in the blood would have a substantial absorption potential for argon radiation.

A coagulation effect was observed in a 5 per cent blood agar solution with a flux of 0.80 watt-seconds, similar to that flux required to affect a 0.01 per cent fluorescein plain agar solution. Mixtures of the various concentrations of fluorescein and blood agar indicate that the absorption potentials of blood and fluorescein are additive in nature, especially at the lower concentrations. Concentrations of fluorescein in plain agar and blood agar above 0.025 per cent appear to offer no enhancement of the photocoagulation effect.

THE SPECTROPHOTOMETRIC ANALYSIS OF BLOOD CONTAINING FLUORESCEIN OR EVANS BLUE

Fluorescein, in a concentration in the blood comparable to that obtained during routine fluorescein angiography of the ocular fundus

(0.01 per cent), produces an increase in absorption (Figure 11) of argon radiation at 4880 Å that is significant (11.6 per cent). The injection of 20 or 30 cc of fluorescein would further increase the absorption of this particular radiation and thereby allow the production of the desired photocoagulation effect with less transmitted energy.

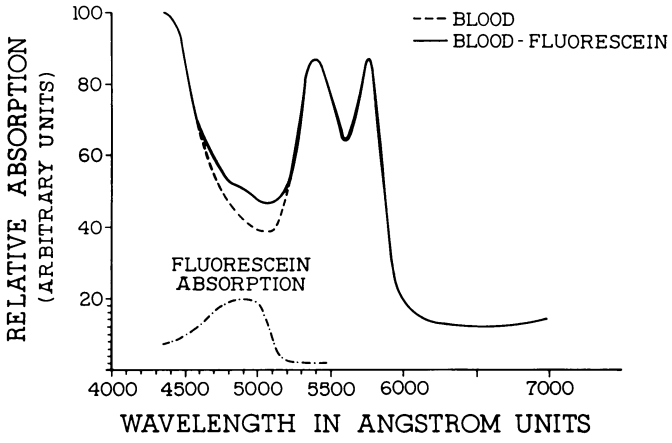

FIGURE 11

The spectrophotometric comparison of human blood and blood containing 0.01 per cent sodium fluorescein showing increased light absorption around the absorption peak of fluorescein (4860 Å), close to one of the principal wavelengths (4880 Å) of argon radiation.

Evans blue can be considered of no practical value as an absorbefacient at a concentration and dosage level that is standard for a blood volume determination (3 cc of a 0.5 per cent Evans blue solution). Further studies are being conducted to determine the practical application at higher concentrations.

Since fluorescein circulates in the plasma portion of the blood column, it would increase the absorption of argon radiation in the capillary bed, and in spaces marked by a paucity of erythrocytes. Furthermore, the leakage of fluorescein into the tissue spaces around injured or abnormal blood vessels should contribute to an increased absorption in these areas. Theoretically, it would be possible to selectively coagulate certain pathologic areas of the capillary plexus by the differential absorption of argon radiation between areas of normal and abnormal permeability.

The Histopathologic Effect of Krypton and Argon Ion Laser Radiation: Animal Studies

During the construction phase of our 10-watt argon laser, we were graciously allowed to use the facilities of the Bell Telephone Laboratories. At these laboratories, working in association with Dr. Edward F. Labuda and Mr. August M. Johnson, we utilized a 2-watt ion laser equipped with a vacuum station capable of producing radiation at all wavelengths of the krypton and argon laser emissions. The radiation at the various wavelengths was constantly monitored at selected intervals with an Eppley Laboratory thermopile that was connected to a Hewlett-Packard Voltmeter, Model 412A. Direct readings were taken at the point of entrance of the beam into the animal's eye, and the power levels were constantly maintained at either 12, 20, or 40 milliwatts, depending upon the particular investigation. The laser radiation was generated in a multi-mode configuration with the beam diameter varying between 2.0 and 2.5 mm. The spectral wavelength emitted by the laser during any particular experiment was measured with a Bausch and Lomb Monochromator to insure a monochromatic beam at the desired frequency.

Thirty-six gray chinchilla rabbits, weighing between 2 and 4 Kg, were used to investigate the histologic effect of krypton and argon ion laser radiation upon the chorioretinal structures. The pupils were dilated maximally with phenylephrine hydrochloride 10 per cent (Neosynephrine) and cyclopentolate hydrochloride 2 per cent (Cyclogyl). Intravenous pentobarbital sodium was used for general anesthesia and was supplemented by the topical application of proparacaine hydrochloride 0.5 per cent (Ophthaine). All rabbits were retinoscoped to eliminate those with any degree of ametropia. Irradiation of the fundus of the rabbit was completed as soon after anesthesia and retinoscopy as possible. The laser beam was swept across the rabbit fundus at a constant rate of about 20° per second creating 10 to 15 parallel coagulations. Ophthalmoscopic examinations were done at the termination of each coagulation session and the fundus of each eye was photographed immediately with a Nikon fundus camera. The condition of the cornea, extent and depth of retinal coagulations, and the effect on choroidal and surrounding retinal tissues were noted. A sketch of the animal's fundus with the area of coagulation was drawn for orientation in future cutting and sectioning of the eye.

The rabbit eyes were photographed and enucleated at selected intervals of one day, one week, three weeks, and, in several cases, six

weeks. The enucleated eyes were immediately fixed in 10 per cent formalin solution. After thirty-six hours the calottes were removed and the central segment returned to the solution. Dehydration was followed by paraffin impregnation, microtome sectioning, and staining with hematoxylin and eosin. Approximately 30 to 50 sections of each eye were examined microscopically to select those sections showing minimal laser damage. The scope of this particular investigation was entirely qualitative in nature designed to determine the portion of the retina or choroid that would be selectively affected by suprathreshold monochromatic light from the representative wavelengths of the krypton and argon CW ion lasers.

KRYPTON ION LASER

The krypton ion laser is capable of emitting radiation in any one of ten different wavelengths. The strongest wavelength emissions, however, appear to be at 6471 Å, 5682 Å, and 5308 Å. These particular strong wavelengths represent ideal examples of continuous laser light in the red, yellow, and green portions of the visible spectrum. Therefore, these spectral lines were used to irradiate the rabbit fundi in addition to the blue and violet lines of the argon laser to be mentioned subsequently. The histopathologic results will be mentioned in groups designated by the wavelength of the laser emission, the incident power level, and by the time of enucleation after irradiation.

Krypton—λ6471 Å—One day—20 milliwatts

GROSS. Pearl white streaks across the rabbit's fundus were observed surrounded by a thin zone of grayish retinal edema. No pigment disturbances or choroidal changes were seen in any coagulated areas. There appeared to be no relationship between the edematous retinal changes and the underlying choroidal pigment pattern.

MICROSCOPIC. Perhaps the most striking effect at this wavelength of radiation is the marked edema of the nerve fiber layer and the internal limiting membrane as well as a moderate disruption of the ganglion cell layer. There are mild vacuolization, disorganization, and coagulative changes in the inner nuclear layer and outer plexiform layer. The outer nuclear layer showed marked edema, coagulation, and derangement of the outer portion with palisading of the bipolar cells. An intense coagulation "meatball" lesion was noted at the junction of the nuclear layer and the rod and cone layer presumably in the region of the cone nuclei. There was considerable herniation and protrusion of the outer cells of the outer nuclear layer into the rod and cone layer

possibly as a result of thermal expansion of these cells. The inner portion of the rod and cone layer in the region of the ellipsoids was heavily affected but the outer areas remained intact. There was marked pigment epithelial response with edema, proliferation, and plication of the pigment epithelial layer. The choroid appeared to be edematous, with some swelling of the vessel walls and moderate hyperemia of the impact area. There was no bulging or buckling of the retinal tissues at this power level.

Krypton—λ6471 Å—One day—40 milliwatts

GROSS. (Figure 12) The orange fundus appeared streaked with white "cake icing" that was much more intense than noted at the 20-milliwatt

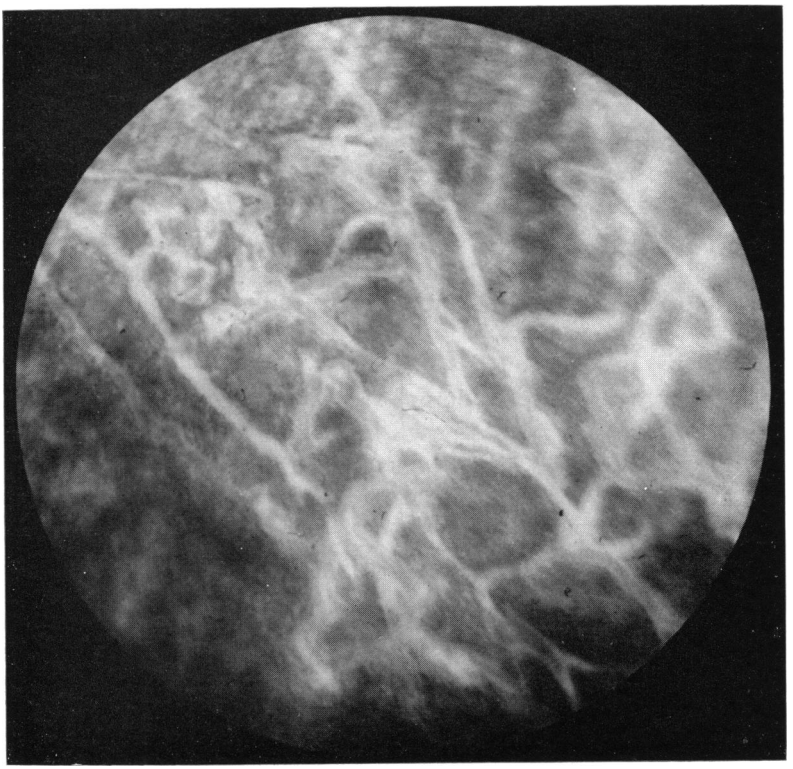

FIGURE 12

Wavelength 6471 Å—40 milliwatts incident corneal power—one day after irradiation: gross appearance of the rabbit fundus showing filamentary streaks of edematous retina along impact zones.

level. Several choroidal areas have been partially blanched along the path of the beam. The retinal coagulation is more demarcated with very minimal surrounding retinal edema and no pigment response.

MICROSCOPIC. (Figure 13) At the higher levels there was an accentuation of all the histopathologic changes noted at the lower power input with the addition of considerable convex bulging, fracturing, splitting, and cyst formation in many areas internal to the rod and cone layer.

Krypton—λ6471 Å—Seven days—20 milliwatts

GROSS. Ophthalmoscopically, the fundus of the rabbits at this time interval showed a fine latticework of pigment lines without any choroidal involvement. Pigment appeared to be proportional to the duration of treatment with some of the pigment lines heavier than others. There were suggestions of a secondary pigment accumulation which ran parallel to the heavy pigment lines but this pigment accumulation was intermittent and extremely wispy. There was no evidence of retinal gliosis, contracture, or other signs of gross retinal disturbance.

MICROSCOPIC. (Figure 14) Histologically, the changes at this wattage level were noted in most of the individual layers of the retina. The nerve fiber and ganglion cell layers showed increased eosinophilic staining and some slight changes suggestive of retinal edema. The inner nuclear layer demonstrated typical changes of coagulation, shrinkage, and coalescence of the cells in that layer. The outer plexiform layer had become deeply eosinophilic with gliotic changes present. The outer nuclear layer had been destroyed in the area of irradiation, and scar tissue had replaced most of these particular cells. Several melanocytes were evident in the area near the junction of the outer plexiform layer and outer nuclear layer. The nuclear layers and the intervening outer plexiform layer were bound together in a semi-structured mass of gliotic tissue. The receptor elements were partially fragmented and disrupted. The pigment epithelium had been stimulated to a moderate degree with resultant proliferation of the pigment epithelium and migration of the melanocytes inward toward the nuclear layers. The choroid was mildly hyperemic with a suggestion of mild hypertrophy and proliferation of the pigment cells in that layer.

Krypton—λ6471 Å—Seven days—40 milliwatts

GROSS. The gross appearance of the irradiated fundus showed that the white edema previously seen had disappeared, and had been replaced with a fine pigment line that was surrounded by areas of choroidal blanching. In several portions of the fundus, there was a

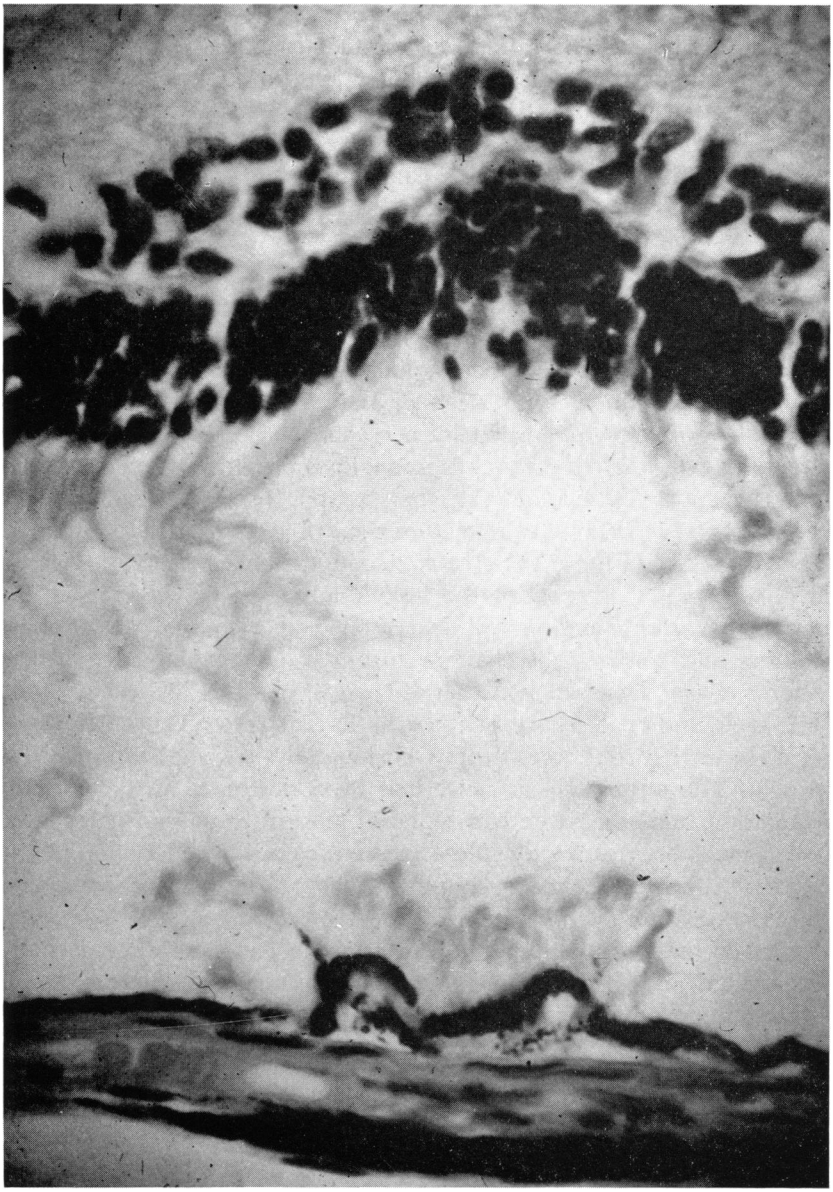

FIGURE 13

Wavelength 6471 Å—40 milliwatts incident corneal power—one day after irradiation: microscopic appearance demonstrating marked pigment epithelial response with minimal nuclear layer change.

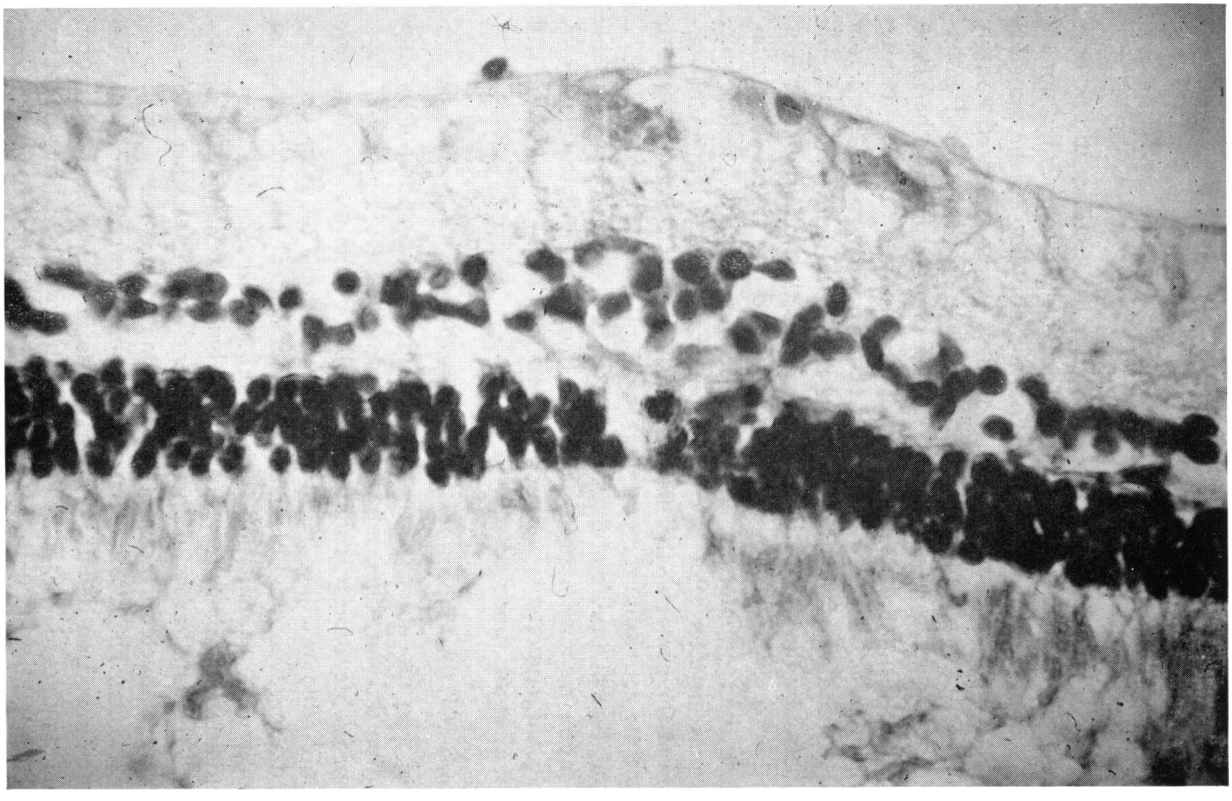

FIGURE 14

Wavelength 6471 Å–20 milliwatts incident corneal power–seven days after irradiation: microscopic appearance showing coagulation and coalescence of outer nuclear and plexiform layers.

suggestion of a prominent pigment accumulation along the beam path with a fainter pigment line on both sides of the heavy line. Choroidal blanching appeared more pronounced in areas where the "railroad track" pigment lines were evident. The larger choroidal vessels appear to be unaffected at this time.

MICROSCOPIC. The microscopic appearance of sections at this time showed that the nerve fiber layer appeared histologically normal although there still was some swelling and stippling of the ganglion cells. The inner plexiform and inner nuclear layers appeared entirely normal. The outer plexiform layer and outer nuclear layers had undergone complete collapse, gliosis, and relative contracture, and had been replaced by eosinophilic scar tissue with several areas of pale-staining epithelioid cells. The bowing inward of the retina was still apparent with a definite separation and splitting of the rod and cone elements presumably by the production of steam at the time of irradiation. The rod and cone layers were partially disorganized due to this disruption, had lost their orientation, and had become markedly eosinophilic. There was an interesting accumulation of proliferated pigment epithelium at the center of the impact area with a relative diminution of melanocytic activity in the peripheral portion of the impact zone. The accumulation of proliferating melanocytes in the impact zone at this wavelength was much more pronounced than at the other wavelengths investigated. Hyperemia and moderate edema of the choroid were still present after this time interval.

Krypton—λ6471 Å—Twenty-one days—20 milliwatts

GROSS. The appearance of the rabbit fundus at twenty-one days after irradiation did not differ substantially from that noted at seven days. Pigment proliferation was slightly more obvious and there was a more definite double or triple line of pigment accumulation along the zone of irradiation. Choroidal blanching was not evident except in areas of heavy pigment accumulation. This would suggest that a heavier dose of irradiation in this area had produced both the pigment accumulation and the small areas of choroidal blanching. The retinal architecture was not affected in areas other than the impact zone.

MICROSCOPIC. The histologic appearance of the rabbit sections at this interval showed no definite changes in the inner layers of the retina. The inner nuclear layer, however, demonstrated slight disorganization, gliosis, and thinning with definite fusion with the outer plexiform layer. The outer plexiform layer had been converted completely to scar tissue in the area of irradiation, and was fused not only to the

inner nuclear layer but also to the inner portion of the outer nuclear layer. The outer portion of the outer nuclear layer had disappeared, owing to a mild coagulative necrosis, and melanocytes were interspersed throughout the periphery of the coagulation zone. Other pigmented cells were seen in the inner nuclear and outer plexiform layers. The rod and cone layer was partially disrupted and showed considerable loss of architecture. No pathologic choroidal changes were noted.

Krypton—λ6471 Å—Twenty-one days—40 milliwatts

GROSS. At the 40-milliwatt level, most of the changes described at the 20-milliwatt level were accentuated. Pigment proliferation was more prominent without the intermittency and beading of the pigment that was apparent at the weaker power level. There was still no observable scarred retina or choroid outside the irradiated areas and healing had taken place without any severe effect upon the vitreous or other ocular structures.

MICROSCOPIC. (Figure 15) Histologically, the nuclear layers were more greatly affected by the irradiation at this power level than at the weaker level. There was considerable disruption, thinning, gliosis, and accumulations of melanocytes within this sector. There was a concentration of proliferated pigment epithelium at the center of the impact areas and the pigment mounds appeared to have migrated into the rod and cone layer. The stimulus to pigment proliferation seemed more pronounced at this wavelength throughout the time intervals studied and especially at the seven- and twenty-one-day intervals noted.

Krypton—λ5682 Å—One day—20 milliwatts

GROSS. Ophthalmoscopically, the fundus of the rabbits appeared streaked with slightly edematous lines that were indistinct and difficult to locate. The zones of coagulation appeared discrete, but the surrounding retinal edema was more diffuse and irregular. There was no change in the pigmented structure of the retina, nor was there any change in the underlying choroidal vascular pattern.

MICROSCOPIC. The most important histologic feature of this wavelength, power setting, and time interval was the edema of the nerve fiber layer and the ganglion cell layer. An additional finding was the swelling of the inner nuclear layer with the propulsion of the cellular elements into surrounding inner layers. In all areas of impact there was a notable widening of the space between the individual cells in the

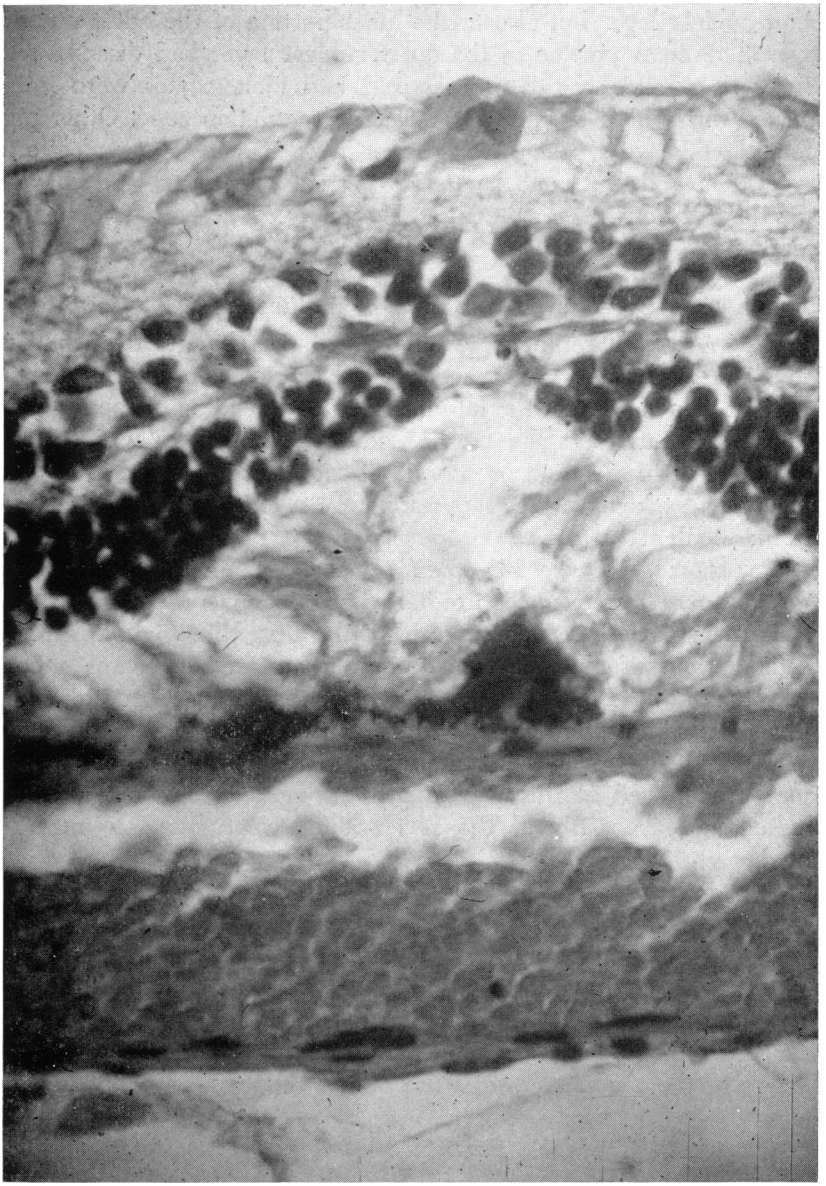

FIGURE 15

Wavelength 6471 Å—40 milliwatts incident corneal power—21 days after irradiation: microscopic section showing marked pigment proliferation, inward bulging of retina, and atrophy of outer nuclear layer.

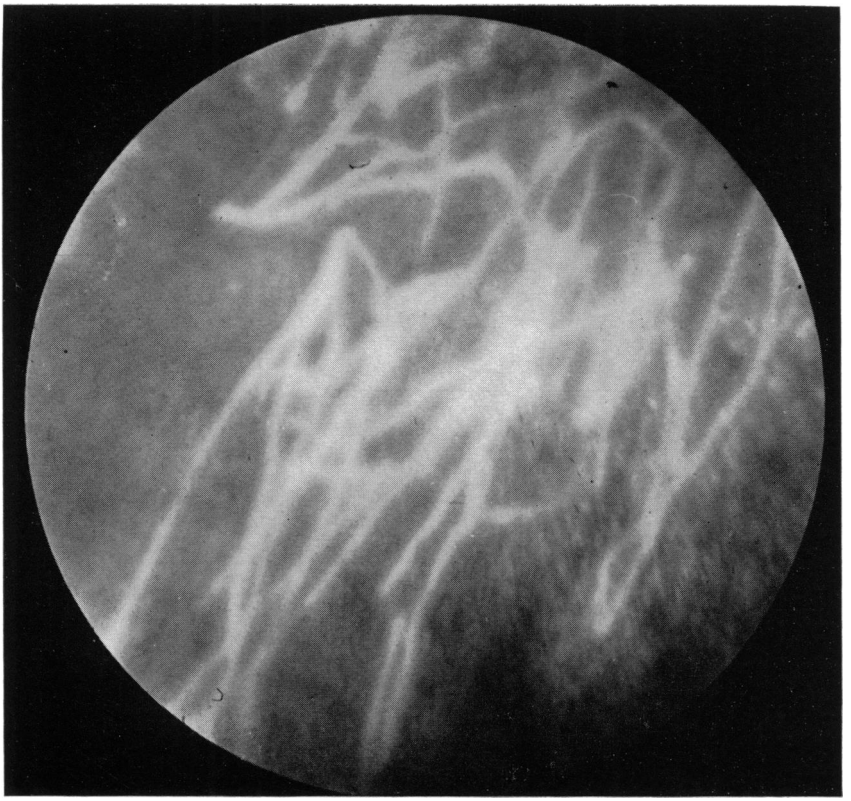

FIGURE 16

Wavelength 5682 Å—40 milliwatts incident corneal power—one day after irradiation: gross appearance of the fundus showing white lines of edematous retina with areas of hazy edema in the intervening retina.

inner nuclear layer with the formation of a modified starburst type of picture. The outer plexiform layer was relatively unaffected at this power level, and the outer nuclear layer seemed totally intact in most of the sections. The receptor elements were not significantly disturbed. The pigment epithelium and the choroid were normal.

Krypton—λ5682 Å—One day—40 milliwatts

GROSS. (Figure 16) The gross appearance of the fundus showed white lines of markedly edematous retina with areas of hazy edema in the intervening retina. There was no demonstrable blanching of the choroidal vessels and no obviously abnormal pigment response.

MICROSCOPIC. (Figure 17) The histopathologic examination showed

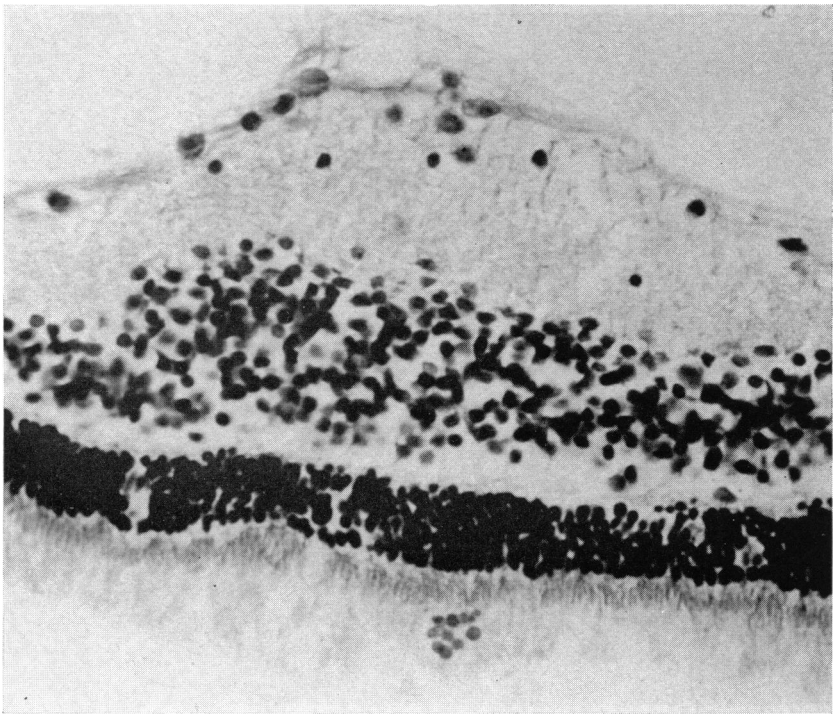

FIGURE 17

Wavelength 5682 Å—40 milliwatts incident corneal power—one day after irradiation: histopathologic appearance demonstrating edema of the nerve fiber layer, ganglion cell layer, and inner nuclear layer. Mild coagulation changes in outer nuclear layer.

marked bleb-like edema of the nerve fiber layer with inward bubbling of the internal limiting membrane and outward bowing of all other retinal layers. The nerve fiber layer was split in several sections and there was slight edema of the cells of the inner nuclear layer. There was a marked focal area of coagulation, collapse, and fusion of the outer nuclear layer and outer plexiform layer, with obliteration of most of the cellular components of the outer nuclear layer. The outer retinal elements, such as the rod and cone layer, pigment epithelial layer, and also the choroidal areas showed little response to this type of radiation.

Krypton—λ5682 Å—Seven days—20 milliwatts

GROSS. Fine pigment lines were present, although more indistinct and zone of irradiation. Each of these pigment lines had a small surround-

ing zone of relative hypopigmentation that made the primary pigment line more prominent by contrast. At the edge of this clearer zone was a secondary piling-up of pigment that was barely visible. Most of these changes were accentuated at the higher power levels. Choroidal changes were not evident.

MICROSCOPIC. These sections were interesting because they showed a definite gliosis and contracture of the outer plexiform layer and the adjacent portions of the inner nuclear and outer nuclear layers. Melanocytes had entered the outer portions of the outer nuclear layer and tiny wisps of melanocytic material extended into the deeper and internal aspects of this layer. Coagulation, necrosis, and gliosis had obliterated large sections of the nuclear layers adjacent to the outer plexiform layer. There was a definite contracture of these layers with a decided pallor and loss of staining ability of the involved cells. Gliotic tissue was arranged in a circular fashion about the nidus of heat production, which seemed to be located at the inner aspect of the outer nuclear layer. There was a mild pigment epithelial response with some proliferation and edema in this layer. The choroidal vascular pattern was unchanged, and appeared normal.

Krypton—λ5682 Å—Seven days—40 milliwatts

GROSS. Fine pigment lines were present, although more indistinct and stippled than those produced by the longer wavelengths. The choroid appeared unaffected, with no suggestion of blanching or blood flow interruption.

MICROSCOPIC. (Figure 18) The sections of eyes irradiated at this time interval and power level showed relatively normal-appearing layers internal to the inner plexiform layer. There was some gliotic activity between the cells of the inner nuclear layer, but the cell bodies themselves appeared unaffected. The outer plexiform layer was the site of intense coagulation changes with disruption, scarring, and agglutination of this layer. The outer nuclear layer appeared to be scarred and slightly contracted, with shriveling of individual rod nuclei near the border of the outer plexiform layer. The rod and cone layer was partially disrupted and disorganized in the region of the impact zone.

Krypton—λ5682 Å—Twenty-one days—20 milliwatts

GROSS. The pigmented lines indicating the areas of treatment were much less pronounced than at the higher power levels. Pigment accumulations could be observed clearly, although they were broken and lacy in many areas. There was some obliteration of the choroidal

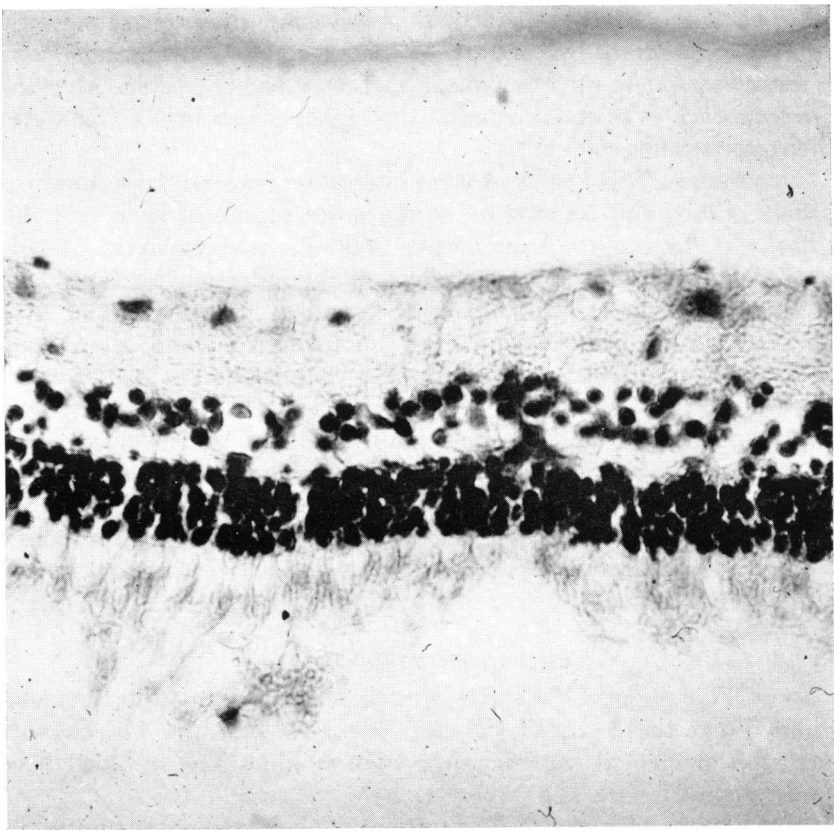

FIGURE 18

Wavelength 5682 Å—40 milliwatts incident corneal power—seven days after irradiation: microscopic appearance showing intensive coagulation, scarring, and agglutination of the outer plexiform layer.

pattern beneath the pigment accumulations, but this was not as pronounced as that noted at the higher powers. There were no obvious vitreal or other retinal changes.

MICROSCOPIC. At this lower power level the most interesting zone of pathology was located in the outer plexiform layer, approximately at the interface between this layer and the outer nuclear layer. A definite circular area of eosinophilic staining material was noted occupying a region approximately the width of the inner nuclear layer. This site of coagulation necrosis, contracture, and gliosis was speckled with several large mononuclear cells with only slight melanocytic activity. Adjacent areas of the outer and inner nuclear layers

stained more heavily, and there was a definite coalescence of the cytoplasm of the cells in these regions. The receptor elements and the outer retinal and choroidal elements were relatively unaffected. Some sections suggested a narrowing of the choroidal vascular pattern, but no occlusive changes could be observed.

Krypton—λ5682 Å—Twenty-one days—40 milliwatts

GROSS. At this interval, pigment accumulations along the coagulation path were much more marked. Blanching of the choroid was obvious in some areas, starting exactly at the pigment lines and extending in one direction distally. The fundus suggested the appearance of flags of blanched choroid waving from the staffs of pigment.

MICROSCOPIC. (Figure 19). Gliosis and scarring of the sites of injury previously noted at earlier intervals had progressed slightly, but the most marked change was the migration of clumps of melanocytes from the pigment epithelial layer to the region of the outer plexiform layer along the path of the laser irradiation. Large mononuclear cells were also noted in the area of the outer plexiform layer, and it was questionable whether these cells represented amelanotic melanocytes or displaced ganglion cells. In all representative sections at both 20- and 40-milliwatt power levels the histologic picture remained unchanged, with a presumably selective absorption in the region of the outer plexiform layer.

Krypton—λ5308 Å—One day—20 milliwatts

GROSS. Ophthalmoscopic examination showed evidence of fine, faint, white lines along the coagulation path. There was little evidence of surrounding retinal edema, and choroidal changes were insignificant. Pigment hypertrophy and vitreous abnormalities were not seen.

MICROSCOPIC. At this power level there were no pathologic changes internal to the outer plexiform layer. In the outer nuclear layer there appeared to be considerable swelling of the individual cell nuclei, as well as separation of the cellular structures. Much of the interstitial tissue stained more eosinophilic and appeared more prominent than unaffected adjacent sections. At the junction of the inner segment of the rod and cone layer and the outer portion of the outer nuclear layer there was a region of pale staining nuclei that appeared to be fragmented and disrupted. This area seemed to be the location of the heat production, since most areas of the retina buckled away from this particular zone. The inner segments of the rod and cone layer were fragmented near this junction, and were progressively less damaged in

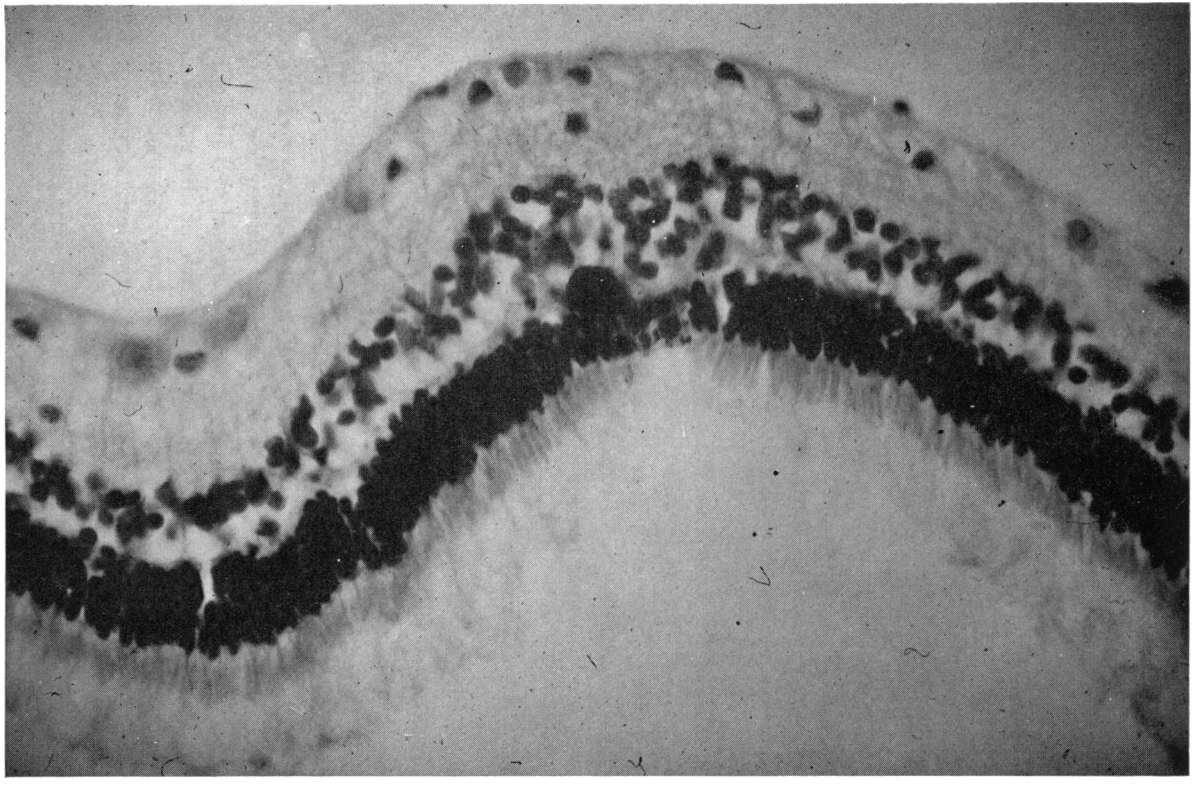

FIGURE 19

Wavelength 5682 Å—40 milliwatts incident corneal power—21 days after irradiation: microscopic section showing large melanocytic infiltration along the path of laser irradiation from the pigment epithelium to the outer plexiform layer.

areas more distant from this zone. The rod and cone and pigment epithelial layers were moderately affected by the radiation with some edema and disorganization. The choroidal vascular pattern appeared to be undisturbed, and was not dilated.

Krypton—λ5308 Å—One day—40 milliwatts

GROSS. (Figure 20) Gross appearance of the rabbit fundus at this interval showed a white icing effect with considerably hazier borders than had been seen with previous coagulations. The intervening retina showed graying and a "waxed paper" appearance possibly due to retinal edema. Choroidal blanching was significant along the lines of the coagulations although the larger choroidal vessels did not appear to be affected.

MICROSCOPIC. (Figure 21) At this wavelength it was notable that the retinal layers internal to the inner nuclear layer were unaffected by the

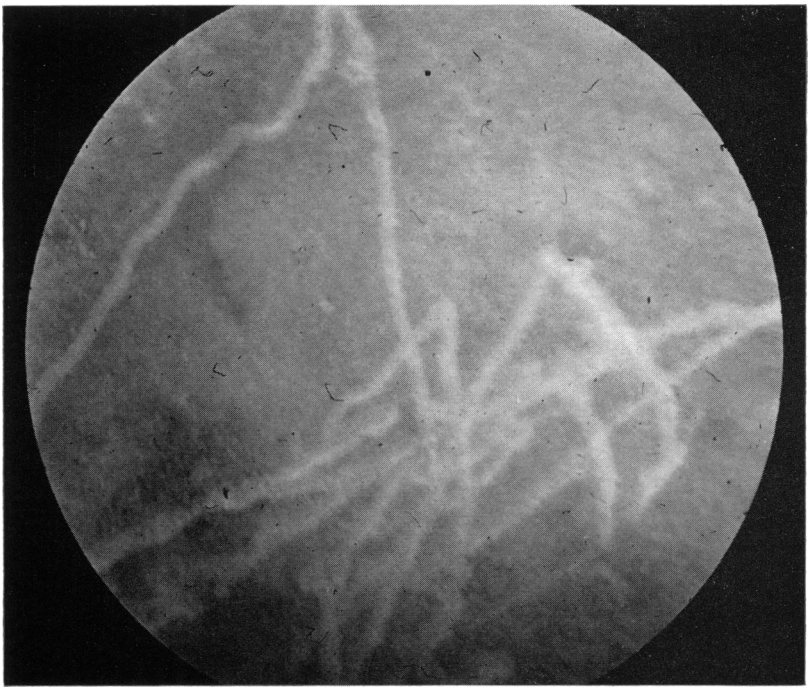

FIGURE 20

Wavelength 5308 Å—40 milliwatts incident corneal power—one day after irradiation: gross appearance of the rabbit fundus showing white "icing" effect of retinal edema along laser path.

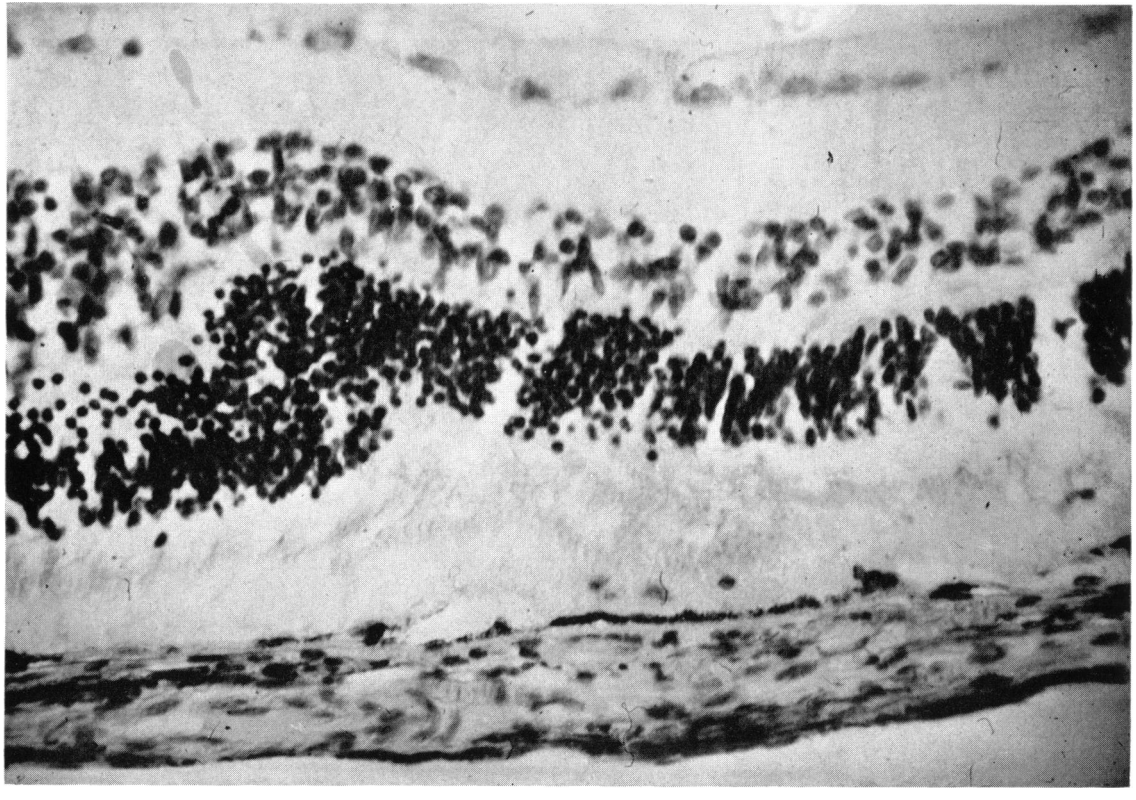

FIGURE 21

Wavelength 5308 Å—40 milliwatts incident corneal power—one day after irradiation: microscopic section showing outer nuclear-receptor layer coagulation zone and splitting of pigment epithelium.

radiation. There was marked edema of the outer nuclear layer, and bowing inward of that particular zone, with some increase in the staining properties of the individual cells. The "meatball" of intense coagulation and absorption of radiation appeared to be located at the junction of the rod and cone layer and the outer nuclear layer. There was disruption of the architecture, intense coagulation, and fragmentation of cells at this juncture. The inner segments of the rods and cones were disorganized, and stained more intensely eosinophilic. The outer segments of the rods and cones did not appear to be affected, although there was blistering and splitting of the pigment epithelial layer in several sections. There appeared to be no choroidal changes at this interval.

Krypton—λ5308 Å—Seven days—20 milliwatts

GROSS. A very fine pigment line could be observed, with a suggestion of a doubling or tripling of these lines. Changes in the choroidal pattern were not observed, nor were there any gliotic changes in the retinal architecture.

MICROSCOPIC. Perhaps the most obvious structural change was the buckling inward of the entire retina. There was little change in any of the layers of the retina with the exception of a mild swelling of the outer nuclear layer. This layer appeared enlarged by approximately 20 per cent when compared with adjacent areas outside the impact zone. The outer portion of the thickened outer nuclear layer showed a very mild disruption of the cell nuclei. The rod and cone segments were not damaged to any extent. The pigment epithelial layer and choroidal layers were all within normal limits.

Krypton—λ5308Å—Seven days—40 milliwatts

GROSS. The prominence of the pigment lines was much more pronounced at this power level. Definite double and triple pigment lines with some residual choroidal blanching were observed.

MICROSCOPIC. (Figure 22) The changes at this power level were more definite, with bowing inward of all layers internal to the outer plexiform layer. A portion of the outer nuclear layer and receptor elements as well as the choroid were buckled outward as though a considerable amount of heat and pressure had been created in the region of the outer nuclear layer and segment junction of the receptor layer. The biconvex buckling of the layers internal and external to the outer nuclear layer produced a cavity which appeared to be lined by a syncytial envelope of coagulated material. Cells adjacent to this

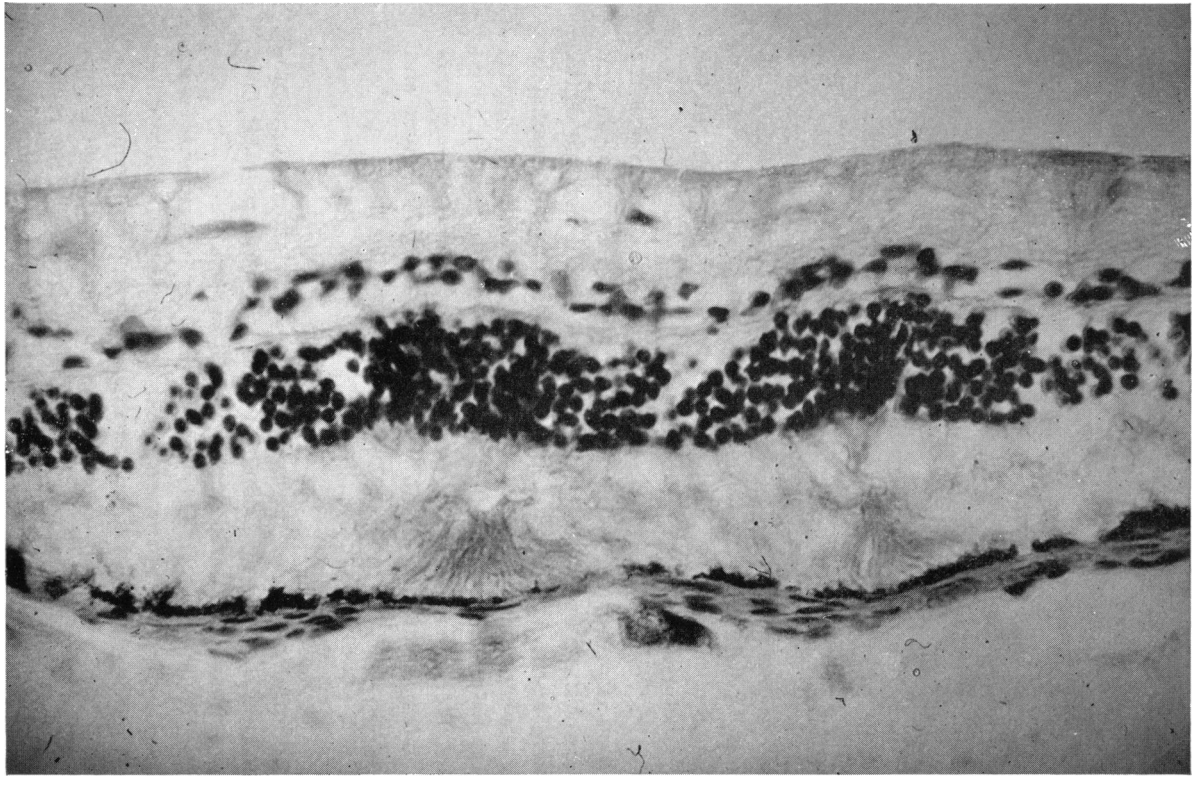

FIGURE 22

Wavelength 5308 Å—40 milliwatts incident corneal power—seven days after irradiation: microscopic appearance showing coagulation and swelling of outer nuclear layer without appreciable pigment epithelial disturbance. Note fan-shaped orientation of receptor elements from heat-producing region at inner-outer segment junction.

syncytial lining were somewhat pale and edematous. All other elements in both the choroid and the retina appeared to be normal in structure and staining properties.

Krypton—λ5308 Å—Twenty-one days—20 milliwatts

GROSS. The triple lines of pigment were striking at this time interval and wavelength. The central dense pigment accumulation probably represented the central zone of laser impact. The two accompanying parallel pigment lines seemed to be located at the border of previously edematous retina and normal retina. Choroidal blanching or vascular alteration was not remarkable.

MICROSCOPIC. (Figure 23) The scarring of the area at the junction of the outer portion of the outer nuclear layer and the inner segment of the rod and cone layer produced marked buckling of the entire retina in these sections. The outer nuclear layer and the rod and cone layer were involved in a large atrophic, contracted cicatrix which seemed to pull the outer portion of the retina together, creating the buckling effect noted. Large clumps of melanocytes were located at the nuclear rod and cone junction, with filamentary extensions of melanocytes running inward in the retina toward the cells in the inner nuclear layer. Again, in these sections, as had been seen in previous wavelength series, the center of increased absorption appeared to be at a definite layer in the retina that eventually determined the disorganization of structure of the surrounding layers.

Krypton—λ5308 Å—Twenty-one days—40 milliwatts

GROSS. The triple distribution of pigmented cells was pronounced, and the retina, in general, was more severely affected than it had been at the lower power level.

MICROSCOPIC. The histologic picture produced by krypton irradiation at this wavelength and power level was dramatic. The layers of the retina from the outer plexiform layer inward were unaffected. However, the outer portion of the outer nuclear layer appeared to be rammed into the rod and cone layer, scattering nuclear layer cells throughout the receptor layer. In several sections, the cells from the outer nuclear layer seemed to have been forced into the rod and cone layer by an explosion originating in the region of the outer nuclear layer. The entire retina was buckled inward from the region of the rod and cone layer either by the force of the initial heat production in that area or by the subsequent edema of the rod and cone layer. Portions of the rod and cone layer adjacent to the outer nuclear layer

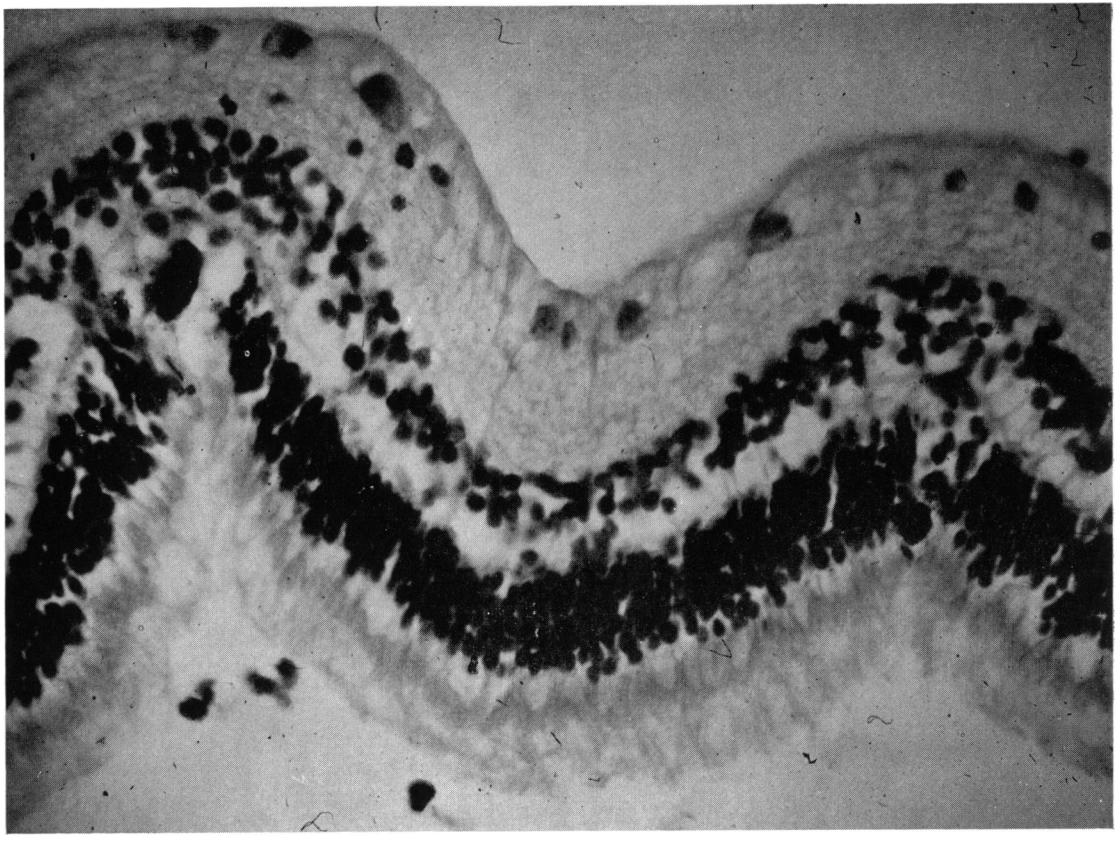

FIGURE 23

Wavelength 5308 Å — 20 milliwatts incident corneal power—21 days after irradiation: microscopic section demonstrating large clumps of melanocytes located at the nuclear-receptor layer junction, gliosis and scarring of these layers, and marked contraction and buckling of the retina.

stained heavily with eosin and had undergone a moderate amount of coagulation necrosis. The choroidal and pigment epithelial layers were not adversely affected. This group of sections demonstrated the selective and destructive coagulation changes produced by irradiation at this wavelength and power level.

ARGON ION LASER

The most intense, and therefore the most useful argon ion laser emission lines appear at 4880 Å and 5145 Å. Since a wavelength near 5145 Å had been previously investigated in the krypton series (5308 Å), it was felt that a study of the 4880 Å line and one of the other seven shorter wavelengths would be most useful. The shortest wavelength produced by the argon laser is the 4579 Å line and this particular emission and the line at 4880 Å were studied for their histopathologic effect on the rabbit retina.

Argon—λ4880 Å—One day—20 milliwatts

GROSS. The coagulation line that appeared on the fundus showed a grayish white, pearly edema that was not as intense as those found at the longer wavelengths. There was some blanching of the underlying choroidal vessels, but this was not as marked as had been seen at other wavelengths. There were no pigment changes, blanching, or edema of the intervening retinal tissues.

MICROSCOPIC. (Figure 24) This study showed a minimal amount of edema of the nerve fiber layer, although the ganglion cell layer and inner plexiform layer appeared completely normal. The matrix surrounding the cells of the inner nuclear layer showed very slight coagulation changes and a suggestion of a slight fusion of this area. There was shrinkage and coagulation of the outer plexiform layer with intercellular bridges of hyperstaining material connecting the inner and outer nuclear layers. There were large, selective, and discrete "meatball" coagulations of edematous tissue containing pleomorphic cells in the central area of the outer nuclear layer. Cells appeared shrunken in some areas and edematous in others with a uniformity in the increased degree of staining of the cellular microstructure. Nuclei were present but appeared indistinct. The primary absorption site appeared to be in the outer nuclear layer, with a thermal overflow striking the junction of the inner and outer segments of the rod and cone layer. A secondary absorption nidus at the junction of the inner and outer segments of the rod and cone layer was apparent, with increased eosinophilic staining in this area and a starburst orientation

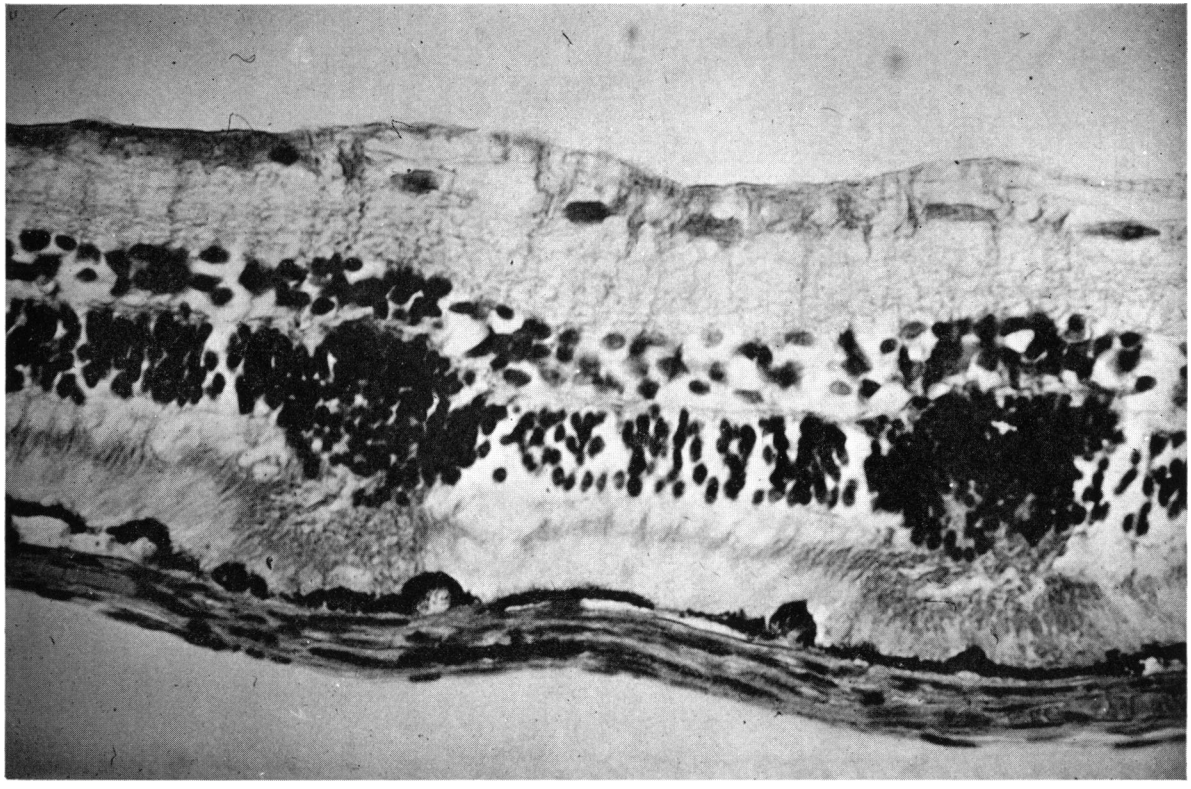

FIGURE 24

Wavelength 4880 Å—20 milliwatts incident corneal power—one day after irradiation: microscopic appearance demonstrating dramatic zones of selective coagulation in the outer nuclear layer and inner-outer segment junction of the receptor layer. Note moderate pigment epithelial response and normal architecture of inner retinal layers.

of the outer and inner rod and cone segments radiating away from the inner and outer segment junction. The outer segments of the rod and cone layers were generally intermeshed in a semistructured coagulation process. The pigment epithelium was slightly edematous, with pigment proliferation and edema more marked at the edges of the lesion. The choroid showed areas of relative hyperemia on both sides of the impact zone.

Argon—λ4880 Å—One day—40 milliwatts

GROSS. The gross appearance at the end of one day at the 40-milliwatt power level showed intense white icing with marked blanching of the large choroidal vessels in most of the coagulation areas.

MICROSCOPIC. Histopathologic sections showed accentuation of all the lesions noted at the 20-milliwatt power level, with the addition of the inward bulging of the entire retina from the nidus of heat production located at the junction of the inner and outer segments of the rod and cone layers. Steam formation had caused vacuolization, splitting, and ballooning of this junction, forcing the large characteristic coagulations in the outer nuclear layer further inward. There was coagulation of the outer segments of the rod and cone layer, and the pigment epithelium demonstrated areas of patchy edema, fragmentation, and blanching in the impact zone. The periphery of the impact site showed hyperpigmentation and proliferation of the pigment epithelium.

Argon—λ4880 Å—Seven days—20 milliwatts

GROSS. (Figure 25) There was a fine speckling of pigment along the coagulation streaks that resembled a faint line of pepper granules. There was some suggestion of tripling of the pigment lines but this was indistinct and not marked. There was no other evidence of scarring of the retina or the choroid, and the choroidal vasculature was entirely intact.

MICROSCOPIC. The entire retina was buckled inward in all zones of treatment. Interestingly, most sections revealed little edema or destructive change in the outer nuclear layer—a prominent feature at higher power levels. The other layers appeared to be within normal limits. The sections that exhibited the most significant changes were the outer segments of the rod and cone layer. Despite the rather remarkable lack of response of the nuclear layers, the junctional area between the outer and inner segments of the rod and cone layer appeared to be damaged irreparably. This region showed considerable coagulation

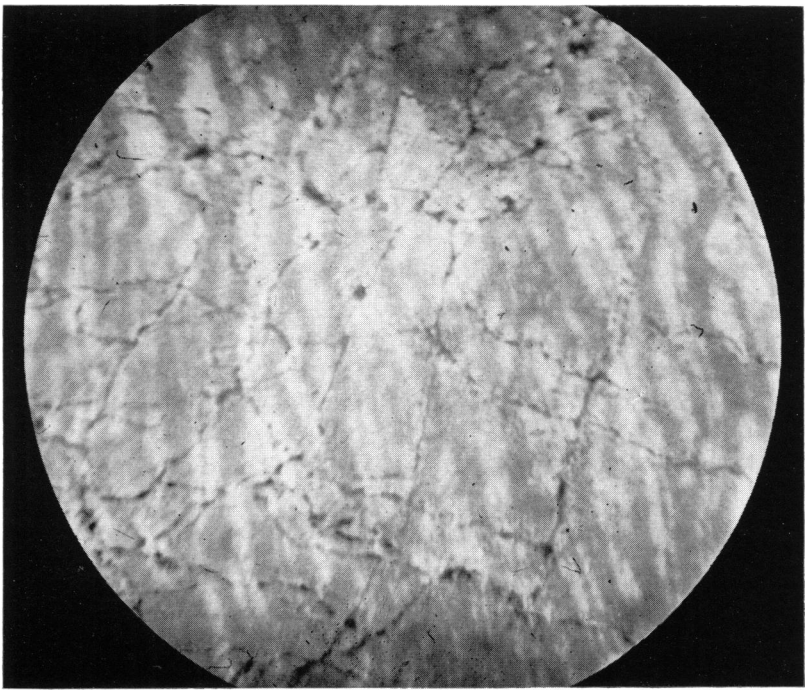

FIGURE 25

Wavelength 4880 Å—20 milliwatts incident corneal power—seven days after irradiation: gross appearance of rabbit fundus showing a fine speckling of pigment along coagulation streaks. Note tripling of pigment lines.

with most of the structures oriented in a fashion that radiated away from the central point of heat production. This particular locus of maximum heat production was situated in the inner aspect of the outer segment of the rods and cones. The entire retina was ballooned and blistered inward like an igloo about a central point. There was mild proliferation in the pigment epithelium and certain portions of the choroidal layers.

Argon—λ4880 Å—Seven days—40 milliwatts

GROSS. Pigment lines representing the paths of coagulation were much more discrete and more pronounced than with the lower power level. The speckled appearance noted at the lower power had been replaced by a moderately broad double and sometimes triple line of pigment with suggestion of pigment hypoplasia between the lines.

Choroidal coagulations and blanching were infrequent and were considered unremarkable at this particular setting.

MICROSCOPIC. (Figure 26) The most interesting facet at this power level and time interval was the retention of the changes produced by the radiation in the outer nuclear layer. As noted, most of these changes were minimal, or had disappeared at the lower wattage. Here it was observed that the outer nuclear cells were disrupted, and there were definite coagulation changes in the interstitial tissue between the individual cellular elements. The other portions of the retina were not adversely affected at this interval, except for the receptor elements. The rod and cone layer was maximally affected by the intense heat produced at the junction of the outer and inner segments. Most of the changes represented an accentuation of the changes found at the 20-milliwatt power level. Buckling of the retina was severe, as were the pigment epithelial and choroidal changes.

Argon—λ4880 Å—Twenty-one days—20 and 40 milliwatts

The gross and microscopic examinations at these particular power levels represent different degrees of the same process affecting the same cellular components. Edema had disappeared in most layers leaving only disrupted and bizarre areas of the eosinophilic scar tissue. Most of the scarring was confined to the region of the outer nuclear and outer plexiform layers at the higher power level, although this was only minimal at the lower power level. The destruction and disappearance of the receptor elements at 40 milliwatts (Figure 27) was also clearly increased over that at 20 milliwatts. Perhaps the most significant difference between the two power levels was the number of melanocytes that had migrated into the nuclear layers, with wisps of pigmented material extending as far inward as the ganglion cell layer. Proliferating melanocytes were apparent at the lower power level, but the amount and distribution were definitely restricted. Buckling of the retina was apparent in all sections at both power levels; the amount of scarring of the nuclear layers directly influenced the amount of residual buckling of the other retinal elements. In all histologic sections at the higher power levels there was collapse, contracture, and scarring of the inner and outer nuclear layers with partial obliteration of the outer plexiform layer. This particular picture was more marked in some sections but was prominent in all. The pigment epithelial and choroidal response was evident at both power levels, but was more obvious at 40 milliwatts.

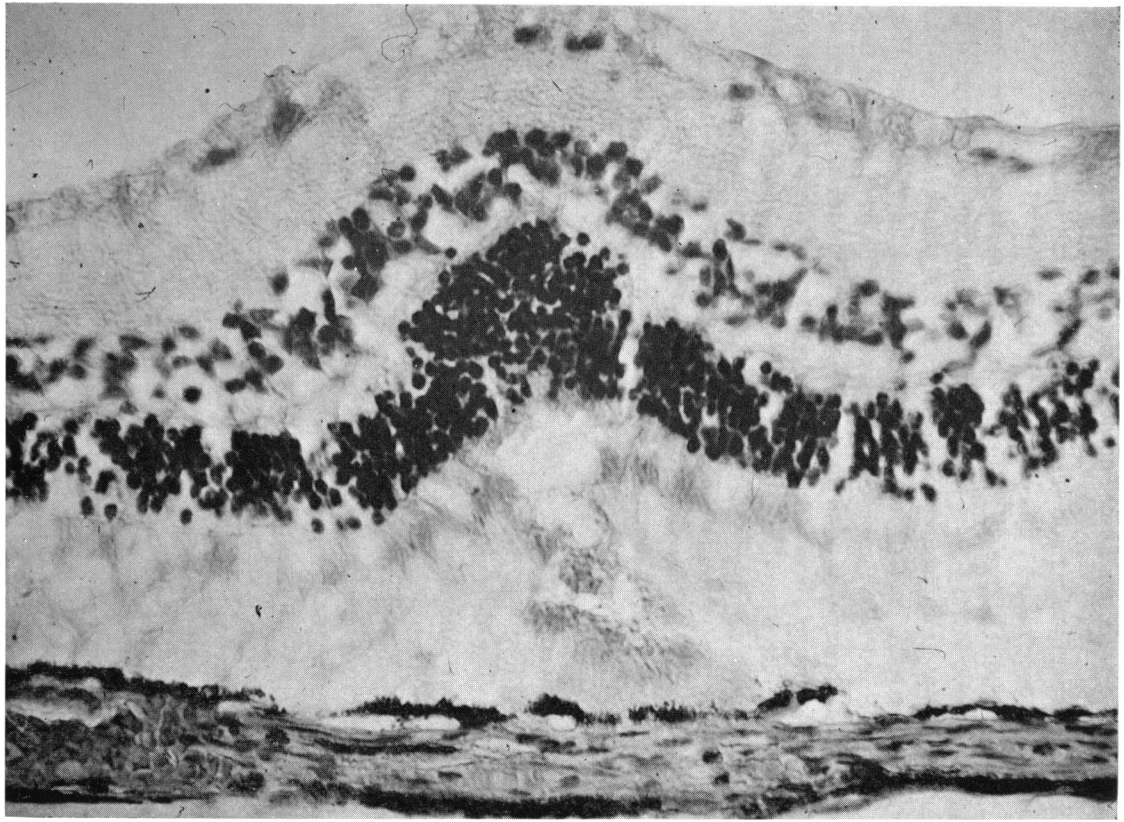

FIGURE 26

Wavelength 4880 Å — 40 milliwatts incident corneal power — seven days after irradiation: microscopic section showing coagulation changes in the outer nuclear and receptor layers with moderate proliferation of the pigment epithelium.

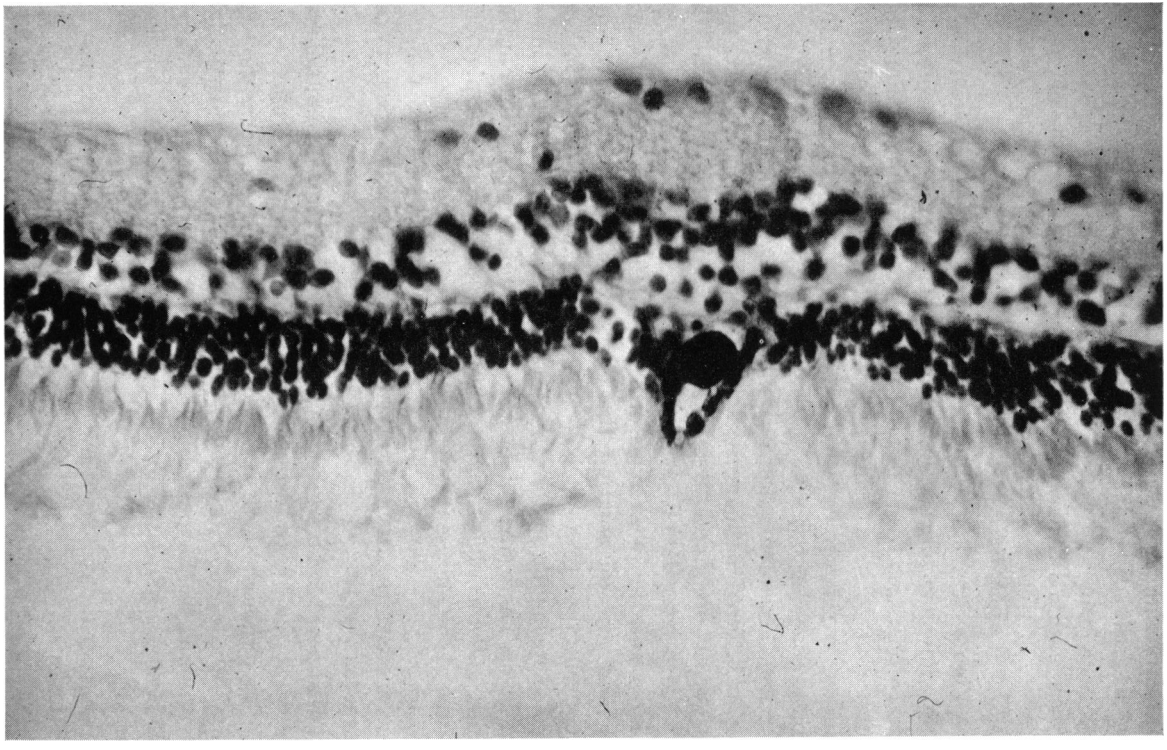

FIGURE 27

Wavelength 4880 Å—40 milliwatts incident corneal power—21 days after irradiation: microscopic appearance demonstrating clumps of melanocytes, scarring, and gliosis of outer nuclear and receptor layers.

Argon—λ4579 Å—One day—20 and 40 milliwatts

The gross and microscopic appearance (Figure 28) of the coagulations were very similar to those described at the 4880 Å wavelength. The most extensive coagulation zone was located at the junction of the outer plexiform and outer nuclear layers. The receptor layer response was minimal with only slight disorganization of the elements.

Argon—λ4579 Å—Twenty-one days—20 and 40 milliwatts

GROSS. (Figure 29) The appearance of the fundus was extremely interesting and showed coagulation lines that were represented by double and sometimes triple lines of pigment accumulation along the coagulation route. These "railroad track" accumulations of pigment corresponded to the proliferation in the pigment epithelium at the border of the coagulation zone.

MICROSCOPIC. The microscopic examination showed normal-appearing retinal layers internal to the inner nuclear layer. The inner and outer nuclear layers were fused and disrupted by contracture of scar tissue. The area of intense coagulation was located at the junction of the outer nuclear layer and the outer plexiform layer (Figure 30). There were many melanocytes surrounding the characteristic "meatball" coagulation core, with the appearance of melanocytes in both nuclear layers, and wisps of melanotic material extending inward as far as the inner plexiform layer. There was absence of all rod and cone structures at the impact site, and the pigment epithelium exhibited increased pigment proliferation at the margins of the irradiated zone.

CONCLUSIONS BASED ON THE HISTOPATHOLOGIC STUDY OF THE EFFECTS OF ION LASER IRRADIATION

1. There appears to be a greater response of the pigment epithelium and choroid at the longer wavelengths (6471 Å) than at the shorter wavelengths, although there was a definite increase in absorption in the region of the 4800 to 5400 Å radiation band. This particular area corresponds to the peak of the pigment absorption curve, and may have been an influencing factor in the pigment epithelial response in this region.

2. Most absorption sites were located at cellular boundaries or cellular interfaces.

3. Edema of the nerve fiber layer and the ganglion cell layer occurs more markedly at the longer wavelengths. This edema is only transitory and disappears at all wavelengths in four to six days.

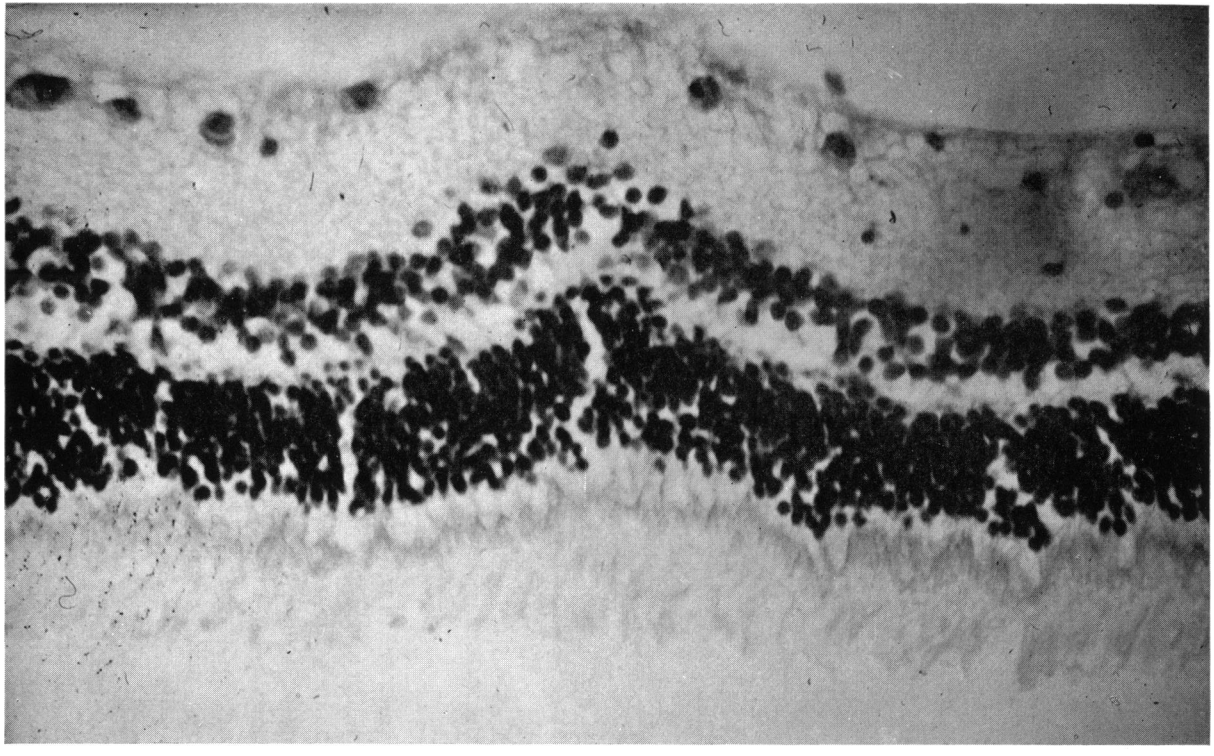

FIGURE 28

Wavelength 4579 Å—20 milliwatts incident corneal power—one day after irradiation: microscopic appearance showing a coagulation core at the junction of the outer plexiform and outer nuclear layers. The receptor layer is relatively undamaged.

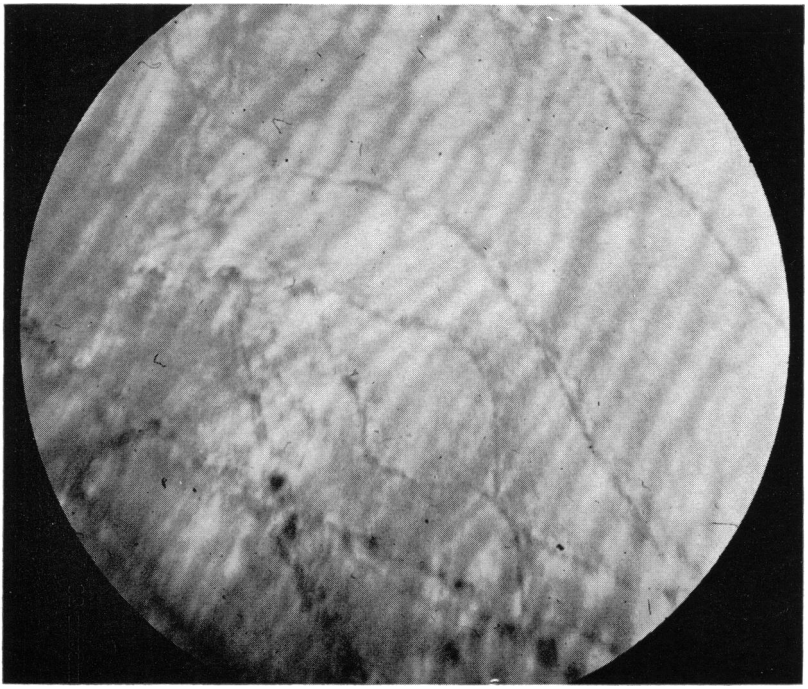

FIGURE 29

Wavelength 4579 Å—40 milliwatts incident corneal power—21 days after irradiation: gross appearance showing double and triple lines of pigment accumulation along the coagulation streaks.

4. The inner plexiform layer was relatively unaffected by any of the wavelengths investigated during this study.

5. The inner nuclear layer was affected minimally and equally by all wavelengths investigated.

6. The outer plexiform layer appears to be most easily affected by heat production in the nearby nuclear layers, especially the outer nuclear layer, and becomes contracted, collapsed, and cicatricial in less than one day.

7. The outer nuclear layer is involved maximally by all wavelengths, usually at the interfaces (except 4880 Å), and absorption is higher than in other non-pigmented cellular structures.

8. The interstitial tissue is affected quickly and more easily than the cells of the nuclear layers, causing scarring and eventual constriction and death of the cellular bodies in these adjacent nuclear layers.

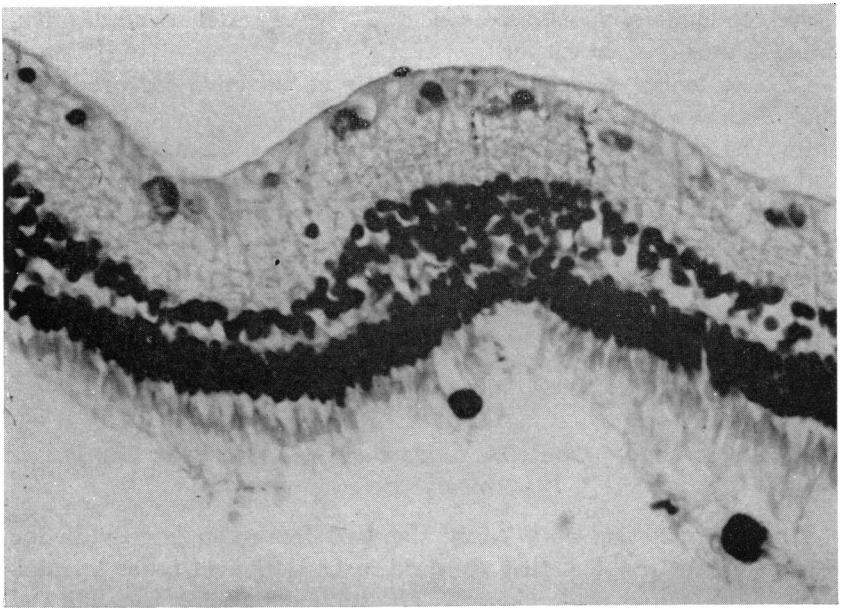

FIGURE 30

Wavelength 4579 Å—40 milliwatts incident corneal power—21 days after irradiation: microscopic section showing melanocytes, pale staining cells, and glial tissue at junction of outer plexiform and outer nuclear layers.

9. The inner segment is more easily affected by heat than the outer segment of the rods and cones.

10. There appears to be a definite absorption zone for the shorter wavelengths at the junction of the inner and outer segments of the rods and cones.

11. Bulging inward of the retina is usually due to the accumulation of heat and the production of steam in the rod and cone layer, sometimes creating edema and thermal damage in the outer nuclear layer.

12. Melanocytes migrate along Müller's fibers with the greatest accumulation of pigment at the zone of greatest damage or heat production. Melanocytes extend away from that zone toward the inner retinal layers along the path of irradiation, diminishing progressively with the distance from the nidus of coagulation.

13. Choroidal effects, both gross and microscopic, are more evident at the longer wavelengths.

14. The shorter wavelengths are least apt to hinder peripheral

nerve-conduction impulses, because of the lack of edema and disorientation of the nerve fiber layer.

15. The longer wavelengths appear more effective for producing chorioretinal adhesions.

16. The cicatricial contracture of the inner nuclear, outer plexiform, and outer nuclear layers in order to occlude therapeutically the deep vascular plexus can be accomplished by any wavelength, but histologically the coagulation is more selective utilizing the shorter wavelengths. Considering the absorption characteristics of hemoglobin for the shorter wavelengths, it would appear that this region of the visible spectrum is definitely preferable for therapeutic vascular coagulations.

The Threshold of the Retina to Damage by Argon Laser Energy: Animal Studies

The determination of a safety standard for argon laser radiation was an urgent problem that required investigation in order to minimize the potential ocular hazard. The unique focusing capability of argon radiation and the associated power level that could be produced in the laboratory made it imperative that the energy required to create an irreversible retinal lesion be measured accurately. Furthermore, the documentation of the retinal power density required to produce a minimal threshold lesion would serve as a basis for the future therapeutic application of argon radiation in diversified biological and medical systems.

INSTRUMENTATION AND METHOD

An LG-12 argon ion laser was employed as the source of radiation. This particular laser had the capability of producing 1.5 watts of radiation in a single transverse mode with a beam divergence of less than one milliradian. During this study, the full beam potential was utilized that included eight transitions ranging from 4579 Å to 5145 Å. The predominant wavelengths, 4880 Å and 5145 Å comprised 90 per cent of the power output. Most of the experimentation was conducted at power levels between 100 and 500 milliwatts exit energy from the laser and the 4880 Å transition was considered to be the spectral line with the greatest power. The argon beam measured 1.2 mm in diameter at the half power point and was determined to be Gaussian in nature during frequent testing.

The auxiliary refinement and manipulation system through which

the argon beam was introduced consisted of a series of optical and mechanical elements, as diagramed in Figure 31. The argon beam was attenuated by Bausch and Lomb neutral density filters that provided a reduction factor between 2 and 1024. The beam could be further altered more precisely by the adjustment of the anode current between 8 and 12 amperes. Although any power below the maximum limit of the laser was attainable, the experimental level seldom varied outside the range of 100–200 milliwatts.

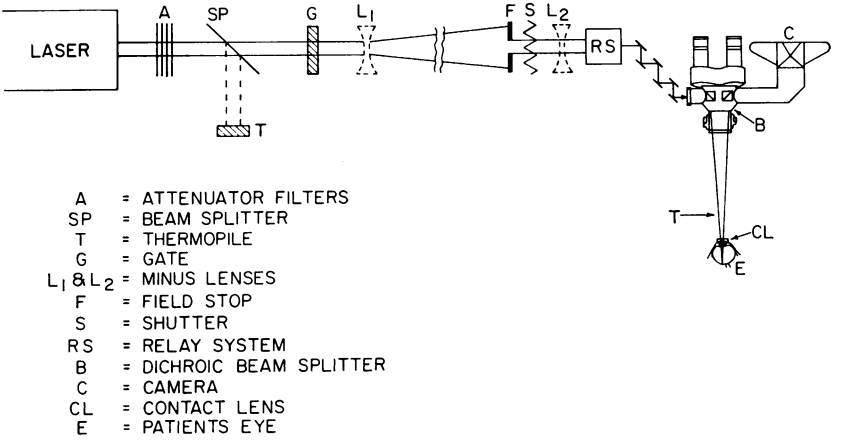

FIGURE 31

Diagram of the optical elements and instrumentation used in the determination of retinal damage thresholds for argon radiation.

A 2 per cent beam splitter was introduced immediately after the attenuation filters, and the deflected energy was directed upon a solar cell that had been previously calibrated by the Bell Telephone Laboratories. The energy was read directly on a Hewlett-Packard Model 201-A voltmeter; this value represented a close estimation of the total energy that was being introduced through the optical system. With this instrumentation, the desired energy levels could be quickly produced by the operator of the laser without interruption of other personnel involved in the experimentation.

The beam next impinged upon a trigger gate that consisted of a nine-decibel attenuation filter connected to an electrically operated relay. This device permitted approximately ⅛ of the total energy to be transmitted along the optical path to the fundus of the test animal. The resulting spot in the animal's fundus could be directed and focused

as necessary, but the transmitted power was insufficient to create an observable lesion. In this way, the delicate portions of the optical apparatus, such as the shutter mechanism, were protected from the full power of the test beam until a moment before the actual coagulation. At this time, the technician responsible for the operation of the shutter mechanism could actuate the relay that lifted the filter from the path of the beam, trip the preset shutter, and return the filter to the path of the beam. The interposition of the filter in the beam also restricted the amount of potentially hazardous energy that coursed along the optical path during the alignment period.

After passing through the trigger gate, the beam was diverged slightly by a −1.00-diopter biconcave lens. This lens was placed one meter from the modified biomicroscope, so that the diameter of the beam at that point was approximately 4.5 mm. The expansion of the beam in this fashion permitted the selection of a small portion of the flattened peak of the Gaussian wavefront that would be relatively free of the typical "hot spot." A field stop with a circular diameter of 2.5 mm was located near the biomicroscope and transmitted the beam onto the shutter element. This Synchro-Compur shutter had been calibrated accurately from one second to 1/500th of a second. Beyond the shutter, a −1.00- or −2.00-diopter biconcave lens was used during certain portions of the study when image sizes larger than those created and determined by the optical properties of the cycloplegic animal's eye were required. The minus lens simply diverged the beam so that it occupied a larger area upon the fundus of the test subject. However, most of the results were obtained at the smaller image sizes produced without the interposition of the ancillary lens.

The entrance aperture of the articulated-arm delivery system intercepted the beam from the shutter device. The reflected beam was then conducted into the biomicroscope and reflected from the dichroic prism through the objective of the biomicroscope (Figure 32). The converging beam was then focused upon the fundus of the animal by direct observation. Such precise focusing was accomplished by neutralizing the corneal surface of the animal with a suitable Lo-Vac contact lens with a plano front surface. The angle of incidence of the argon beam upon the front surface of the contact lens was held constant within 10°. Refocusing upon different portions of the paramacular area of the monkeys and the clear retinal area of the rabbits was performed before each coagulation. The beam size was estimated by means of a micrometer eyepiece in the biomicroscope that had been calibrated against needles of known size in air and against the vitreal-retinal face of the actual test animal. The beam diameter at the site

FIGURE 32

Photograph during retinal threshold determinations, showing articulated arm and surgical biomicroscope coupled to permit delivery of the argon beam into the rabbit's eye.

of impact was considered equal to the average of the fluorescing spot size as seen through the anti-argon ocular filter and the somewhat indistinct and scattered beam size as observed directly. The lesion size was also measured at various intensities and compared. Final energy measurements were taken after each coagulation by placing the absorbent cone of an Eppley thermopile at a position directly in front of the animal's contact lens. In this manner, the actual power incident upon the contact lens was obtained after passage through the rest of the optical system. The calculation of retinal impact energy and power density was obtained by deducting the reflection and absorption losses of the contact lens and the ocular media absorption loss of the test animal from the incident energy measured by the thermopile. The actual image areas were calculated and the threshold levels were recorded in watts per square centimeter of chorioretinal tissue. A threshold lesion was considered to have been produced when a demonstrable morphologic change, however slight, could be observed within one hour after impact. Fundus sketches and photographs with a Nikon fundus camera were made at appropriate intervals so that an accurate correlation of the various parameters could be readily compared for statistical use.

Gray chinchilla rabbits weighing between two and four kilograms and rhesus monkeys weighing between two and three kilograms were employed in these animal experiments. Anesthesia was achieved in the rabbits by the intravenous injection of pentobarbital sodium (Diabutal) and the pupils were dilated maximally with 2 per cent Cyclogyl and Neosynephrine 10 per cent. In several instances the monkeys were tranquilized with injections of Sernyl (1 mg/lb. intramuscularly) prior to injection with pentobarbital sodium (3 to 4 mg/lb. intravenously). Small lateral canthotomies were necessary in the monkeys in order to insert the contact lens. A solution of isotonic saline was used to irrigate the corneas when necessary.

The following system of operation was used by the personnel involved in the threshold investigation. The specially modified biomicroscope was used to examine the fundus of the animal eye and to focus accurately a weak argon beam upon a suitable target site. Because the animal was lying motionless on the surface of the table, little refocusing and additional movement of the visualization apparatus were necessary after the primary adjustment. Either the 10-power or 16-power magnification doublet of the Zeiss biomicroscope was employed for accurate observation. When the desired area had been selected and the proper focus had been attained, the first technician

adjusted the power level of the argon beam by varying the attenuator filters and the anode amperage of the laser power supply. A short countdown was then initiated and, at time zero, the second technician raised the nine-decibel attenuation gate that allowed the argon beam to fall upon the field stop and shutter mechanism. The shutter mechanism was immediately triggered at the desired exposure interval, and the attenuation gate was dropped back into its original position. The immediate result of the laser impact was then recorded as an "effect" or "no effect." The location of the impact site was marked and labeled on a suitable retinal drawing for future observation during the ensuing hour. Approximately ten to twelve impacts were performed at each power setting and the results recorded. A new area of the fundus was then selected and the power level adjusted for additional impacts at different power and exposure times. Twenty to thirty test impacts were performed on each animal eye before employing another eye for further investigation.

The energy necessary to create a barely visible threshold lesion within one hour after the time of impact was determined for exposure times of 2, 4, 10, and 20 milliseconds. The actual threshold for a particular exposure was considered to be that power level that would create a lesion 50 per cent of the time in the paramacular area of the monkeys or in the clear retinal area of the rabbits. The numerous impacts of laser radiation were judged to have created an "effect" or "no effect" and were plotted in terms of damage probability for that particular energy level. Damage probability was defined as the number of events in which damage was observed in the interval, divided by the total number of events in the interval. The energy range along the graph was divided into equal intervals, the damage probability was calculated for each range interval, and a histogram was plotted as shown in Figure 33. A smooth curve was then drawn along the average of the probability plotting points throughout the energy scale. The point at which the smooth curve intersected the 50 per cent damage probability line was considered to be the energy required for threshold damage at that particular exposure interval.

CALIBRATION

The calibration specifications and tolerance of the optical elements that were used during this study were unchanged from previous experiments, and represented a high order of accuracy. The thermopile had been calibrated at the Eppley Laboratory for both low (10 mw/cm^2) and high (100 mw/cm^2) entrance energies. The multiple optical lenses

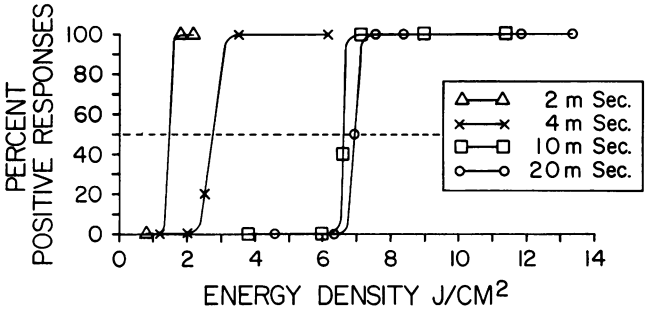

FIGURE 33

Composite of the retinal threshold damage curves for argon radiation. Fifty per cent damage probability curves for exposure intervals of 2 msec. (1.4 j/cm^2), 4 msec. (2.7 j/cm^2), 10 msec. (6.6 j/cm^2), and 20 msec. (6.9 j/cm^2).

and filters, as well as the articulated-arm delivery system, accounted for a slightly larger spot size than theoretically possible with the naked argon laser beam. The plano contact lens used to neutralize the power of the cornea was measured spectrophotometrically and found to absorb less than 1 per cent of the argon light and to reflect approximately 11 per cent at the front surface. Therefore, a 12 per cent decrease in total energy from the measured precorneal thermopile level was expected during transmission of the beam through the contact lens. The ocular media of the rabbit was considered to absorb 10 per cent of the radiation as determined by the studies of Geeraets and his coworkers.[14] The ocular media of the monkeys was assumed to absorb approximately 17 per cent of the incident radiations, using the human values reported in the same article. The energy losses in the contact lens and the ocular media were deducted from the thermopile readings in the final retinal energy calculations. The total error inherent in the optical devices and technique of the investigators was considered to be less than 19 per cent overall in this study.

RESULTS

The following results were obtained from the threshold investigations conducted with the chinchilla rabbits and the rhesus monkeys:

1. The image diameter of the argon laser beam on the rabbit fundus was calculated to be 115 microns in diameter, representing a retinal area of 1.04×10^{-4} cm^2. The image size of the argon beam on the monkey fundus was considered to be 105 microns, or 0.87×10^{-4} cm^2 of retinal tissue.

TABLE 1. THRESHOLD DATA—DAMAGE TO RABBIT RETINA

Image size (μ)	Exposure (msec.)	Corrected for contact lens loss: Incident corneal energy (mj)	Corrected for contact lens loss: Incident corneal power (mw)	Corrected for contact lens and ocular medium losses: Retinal energy (mj)	Retinal energy density (j/cm^2)	Retinal power (mw)	Retinal power density (w/cm^2)
115	4	0.29	72	0.26	2.5	65	625

TABLE 2. THRESHOLD DATA—DAMAGE TO MONKEY RETINA

Image size (μ)	Exposure (msec.)	Corrected for contact lens loss: Incident corneal energy (mj)	Corrected for contact lens loss: Incident corneal power (mw)	Corrected for contact lens and ocular medium losses: Retinal energy (mj)	Retinal energy density (j/cm^2)	Retinal power (mw)	Retinal power density (w/cm^2)
105	2	0.14	74	0.12	1.4	61	700
105	4	0.29	71	0.24	2.7	59	675
105	10	0.69	69	0.57	6.6	57	660
105	20	0.72	36	0.60	6.9	30	345

2. Table 1 represents the threshold energy necessary for a visible retinal coagulation in the rabbit with a 50 per cent probability, during the four-millisecond exposure interval noted. The incident corneal energy prior to impingement upon the contact lens and the retinal energy and power density after passage through the contact lens are also noted.

3. The energies necessary to create a lesion in the monkey retina with a 50 per cent probability during the observation period of one hour at various exposure times are reported in Table 2. Various energy and power densities along the path of the beam prior to entrance into the eye and at the retina are noted also.

DISCUSSION

All laser systems have characteristic features that can be advantageously used in the irradiation of biologic tissue. The inherent properties of continuous-wave lasers permit the beam to be manipulated, regulated, and focused precisely in order to create a more predictable ocular tissue reaction than any existing incoherent radiation. The results of our investigations have supported the contention

that the argon ion laser affects tissue in a manner that depends upon its wavelength, intensity, duration of exposure, and the absorption potential of the irradiated tissue. The exciting physical and biological effects produced by argon laser radiation are discussed in subsequent sections that are applicable only to a unique light source such as the laser. These categories reflect the primary differences between incandescent light sources and laser sources, and in some cases may further differentiate the argon gas laser from other types of lasers.

Specific Target Response

The absorption of high-intensity energy from the visible and near visible portions of the spectrum, with a subsequent degradation into thermal energy, has long been known to be a source of ocular pathology. The work of Verhoeff *et al.*,[9] Eccles and Flynn,[10] Cogan,[11] and Friedenwald and others[12] has emphasized that certain tissues, enzyme systems, and organisms are much more sensitive to some specific wavelengths than to others. Most of the early photobiology literature, prior to the advent of lasers, indicated that the character of light-induced effects on a given material was defined by an action spectrum which correlated well with the absorption characteristics of the biological material used. Experience with laser energy in various biological studies has indicated that similar phenomena are operational.[13,15,16] Investigations have shown that biological damage at those laser frequencies tested is produced in proportion to the amount of energy absorbed by either natural chromophores or dyes. Rounds *et al.*[17] observed that hemoglobin within intact human erythrocytes could be bleached with a wavelength of 5300 Å from a frequency-doubled neodymium laser. An equivalent power density and pulse width produced by a Q-switched ruby laser showed no such bleaching action. Furthermore, his studies showed that the green wavelength (5300 Å) could specifically inhibit the electron-accepting activity of cytochrome C, while wavelengths of 6013 Å and 6096 Å from a Raman-shifted ruby laser produced a similar effect in cytochromes A and A_3 in rat brain cell suspension.[18] This specific wavelength-dependent activity of the cytochrome systems within the internal mitochondrial membranes has been demonstrated strikingly by irradiation with various intense monochromatic laser sources.

The specific pathology of chorioretinal burns resulting from exposure to sunlight,[9] atomic fireballs,[19] and ruby lasers[20,4,2] has been described

previously. In these instances, the pathophysiologic events follow the course analyzed by Vos.[21] His conceptual studies have shown that most of the energy is absorbed in the melanin granules of the pigment epithelium. The granules transfer heat by conduction, convection, and radiation to the proteins around them, which are denatured or coagulated. Investigations of the effect of ruby laser radiation on tissue cultures of pigment epithelial cells have shown that the lethal effect depends upon the number of pigment granules per cell.[22] The reported action of lasers on melanotic cancer cells involves a similar heat transfer from discrete pigment granules to vital cytoplasmic constituents.[23]

The histopathologic studies conducted in our laboratories have explored the effect of low-power radiation from krypton and argon ion lasers on the rabbit retina. Our study was primarily concerned with the qualitative response of the retina to the incident radiation, noting particularly the cells or cellular layers that were damaged by minimum impact energies. Wolbarsht *et al.*[24] have demonstrated that the ruby laser produces radiation that is absorbed primarily at the pigment epithelial layer, whereas the neural portions of the retina absorb more neodymium laser energy (10,600 Å) than the pigment epithelium. In our studies, histologic examinations of the rabbit eyes showed that the damage sites produced by 6471 Å were similar to those at 6943 Å and were confined primarily to the area near the pigment epithelium, with minimal changes in the region near the junction of the outer nuclear layer and receptor layer. However, irradiation with laser energy at 5682 Å produced marked edema of the nerve fiber layer and the ganglion cell layer, considerable coagulative changes and agglutination at the interface of the outer nuclear and outer plexiform layer, and a much milder pigment epithelial response. At the 5308 Å wavelength, the pathologic disruption was located primarily in the outer portions of the outer nuclear layer, with little change in any of the other chorioretinal areas. Irradiation with laser light of 4880 Å and 4579 Å resulted in fusion of the inner and outer nuclear layers, coagulation and cellular coalescence at the junction of the inner and outer segments of the rod and cone layer, as well as slight to moderate proliferation of the pigment epithelium. It appeared that there were definite sites of relative absorption, other than the pigment epithelium, that contributed to the conversion of light to heat energy. From our findings with radiation in the visible spectrum, it was obvious that the nuclear layers, portions of the receptor layer, and certain sensitive cellular complexes were being damaged either by thermal energy produced in

the nearby pigment epithelium or by heat created by the absorption of light energy in the complexes themselves, or a combination of these factors that varied with the incident wavelength.

The exploration of the first premise that the layers of the retina are damaged by heat radiating from the absorptive pigment epithelial cells is interesting. Townes[25] in 1962 theorized that absorbent spheres the size of a pigment melanin granule could produce a rise in temperature of 500° C with an incident laser power density of approximately 4×10^5 w/cm^2. According to Vos' mathematical model of thermal flux, temperatures greater than 100° C were reached in the pigment epithelium for 10 and 0.5 milliseconds, respectively, as a result of a 30-millisecond and a 175-microsecond flash of xenon-arc energy.[21] When the incident xenon-arc photocoagulation burst lasted 30 milliseconds, the region of the ellipsoids was considered to be above 50° C during an interval of 7 to 90 milliseconds. If the same energy was confined to a burst period of 175 microseconds, the area of the ellipsoids reached a temperature exceeding 50° C for only 10 milliseconds. The work of Geeraets and his associates[26] further showed that a microsecond and nanosecond burst of laser or xenon-arc energy produced little histologic damage to the inner layers of the retina, presumably because of the localized production of heat at the pigment epithelium without the time interval necessary for thermal conduction. These authors also noted that the outer nuclear layer was often disrupted and agglutinated during the longer 30-millisecond xenon-arc coagulation. This disruption, they thought, was not due to steam production in the pigment epithelium, since the nuclear layers occupied a region more than 100 microns away from the absorbent melanocytes.

The alternative explanation of the observed phenomenon of nuclear layer coagulation without significant pigment epithelial changes is that certain cells or cellular components may be highly effective individually as primary absorption sites for certain wavelengths. It was shown that the intense coagulation sites occurred on the inner surface of certain cellular layers, such as the outer nuclear layer, with relatively normal-appearing cells between the coagulation zone and the pigment epithelium. At wavelengths below 5682 Å, the pigment epithelial response was much too slight to account for the severe coagulation changes that occurred in the inner retinal layers. Furthermore, it is difficult to explain the gross edema of the nerve fiber layer, the selective starburst orientation of the damage at the inner- and outer-segment junction of the rods and cones, and the relatively undisturbed condition of the

interposed retinal structures without postulating the existence of specific intraretinal wavelength-dependent absorbing tissues or enzyme systems.

Sjöstrand has shown that the photoreceptors of vertebrates are made up of outer and inner segments. The outer segments of the rods and cones contain the photosensitive pigments, and the inner segments contain accumulations of mitochondria.[27] The various respiratory enzymes and electron carriers are an integral part of the mitochondrial structure, so that the whole respiratory capacity of the visual cells seems to reside solely in the inner segments.[28] Those parts where such enzymes are lacking must make use of anaerobic mechanisms for their metabolic needs; it has been shown that, in the rabbit and monkey, the outer plexiform layer is rich in glycolytic enzymes.[29] Because of their absorption potential, the cytochrome enzymes must be considered as a possible site of absorption of the incident laser radiation. The outer segment may also play an important role in photon absorption, since many visual pigments have been described in the rods and cones of vertebrate eyes. The photosensory pigments that have been extracted or synthesized include euphausiopsin (λ-max. 463), rhodopsin (λ-max. 497), cephalopsin (λ-max. 491), porphyropsin (λ-max. 522), iodopsin (λ-max. 562), and cyanopsin (λ-max. 620).[30] The most important photosensitive pigments in humans are rhodopsin and iodopsin. Rhodopsin, located entirely in the outer segments of the rods, absorbs radiation maximally in the region of 497 millimicrons, produces nervous energy, and bleaches to a product that has the photometric spectrum of retinene 1. Rounds *et al.*[31] have shown that the dark-adapted rod absorbs a substantially greater quantity of argon laser radiation than the light-adapted rod. It is conceivable, therefore, that the disruption, disorientation, and agglutination that is characteristically present at the junction of the inner and outer segments of the rods when irradiated with argon laser energy could be due to the preferential absorption of this energy by rhodopsin. Iodopsin, although never extracted from the fovea of man, has been postulated to exist by Wald *et al.*[32] who has isolated from the retina of the chicken this photosensitive pigment, which contains almost exclusively cones. Iodopsin resembles rhodopsin in many of its chemical characteristics, but has a λ-max. at 562 mμ. Upon bleaching, this particular photosensitive pigment reverts to a substance that has a peak absorption at 500 mμ. Rushton and his coworkers have determined, on the basis of chorioretinal reflectance studies, that at least two photosensitive pigments

exist in the cones of man, and he has named these pigments chlorolabe (λ-max. 540 mμ) and erythrolabe (λ-max. 590 mμ).[33] It is also of interest that Rounds showed that beta-carotene (retinene), the common carotenoid of the rhodopsin and iodopsin systems, is less light sensitive and has less tendency to bleach to some other substance than its related pigments. Instead, he found that treatment with either the 4880 Å or the 5145 Å wavelengths appeared to convert the mixture of *cis* and *trans* stereoisomers to an all *trans* form of the molecule.[31] This molecular stability, together with its ability to bind with cellular membranes, as demonstrated by Chapman,[34] makes carotene an attractive candidate to explain the wavelength-dependent photocoagulation with the argon laser.

In summary, it would appear from the information available in the literature and the results of our histopathologic studies that the effects of light of various wavelengths upon the retina of the rabbit are due to damage inflicted by the thermal conduction of heat away from the pigment epithelium, and to the primary absorption of radiation in certain retinal layers that contain chromophores receptive to the incident radiation. The proportion of damage created by each mechanism varies with the wavelength of the light energy. The histopathologic results suggest that radiation at 6471 Å is transmitted through the retina with little attenuation, is absorbed primarily at the pigment epithelium, and is conducted as thermal energy to the nuclear layers. At 5682 Å and 5308 Å the erythrolabe or chlorolabe of Rushton, or iodopsin or its bleached product, could provide the necessary photosensitive material to produce the coagulation of the nuclear and receptor layers that is characteristic at these wavelengths. The histologic response at 4880 Å and 4579 Å could be explained by the preferential absorption of incident radiation by either the rhodopsin complex in the outer segments of the rods, or the bleached product of iodopsin in the outer segments of the cones. The increased sensitivity of the pigment granules to radiation at these shorter wavelengths would account for the moderate pigment epithelial response that was noted on histologic examination. Other ill-defined factors such as the pigment sensitivity curve, the shift of photosensitive pigment absorption potentials with scotopic or photopic conditions, the intensity of radiation and its accumulative effect on various layers of the retina, the length of various exposure intervals, and the structural variations in carotenoid content in different parts of the retina also probably influence the photochemical or photothermal processes that occur in the retina during irradiation.

Minimum Energy For Desired Effect

The unique qualities and associated ocular hazards of argon laser radiation made it urgent that laboratory safety standards be established. It was essential that values be provided which would specify the maximum laser energy that could be tolerated safely by the retina. Our threshold and blood studies have yielded energy density levels above which chorioretinal damage occurs with argon irradiation.

Our investigations have demonstrated that 1.4 j/cm^2 must be delivered to the monkey retina for damage to occur during a two-millisecond period. Additional threshold determinations have shown that 2.7 j/cm^2 of argon energy is necessary during a four-millisecond period, 6.6 j/cm^2 during a ten-millisecond interval, and 6.9 j/cm^2 during an exposure of twenty milliseconds. Three previous publications which have been concerned with the energy necessary to produce threshold coagulations with light of a continuous nature deserve consideration. In the first of these, Ham *et al.*[35] stated that a thermal dose of 0.15 to 0.20 calories per square centimeter delivered in 175 microseconds by a xenon lamp produced a threshold lesion, and they presented additional data to show that certain lasers would have a similar threshold if pulsed at that exposure interval. It is extremely difficult, however, to pulse argon lasers into the microsecond or nanosecond range for the purpose of energy comparison and therefore those data dealing with the threshold levels of pulsed lasers are of no immediate concern. A practical operating interval for argon laser photocoagulation is 250 milliseconds or longer since the entire procedure is conducted under manual control. Nevertheless, it is of interest to investigate the threshold damage level for the short exposure intervals from 2 to 20 milliseconds since Geeraets *et al.*[26] have shown that the total energy necessary for coagulation at these exposures is considerably less than that required for the longer intervals in the practical therapeutic range. Furthermore, the damage level should be measured at an interval that is shorter than the period necessary to activate the blink reflex (150 msec.) in order to assess the laboratory hazard. Investigations using a modified xenon-arc lamp with controlled exposures varying from 175 microseconds to 30 milliseconds have been conducted by Geeraets.[26] His studies showed that minimal retinal lesions were produced at a 30-millisecond exposure with a retinal dose of 4.0 j/cm^2. His figures are comparable with our projected values, if extrapolated to 30 milliseconds (7.2 j/cm^2). Considering the differences in focal length, ocular media absorption, and chorioretinal anatomy between rabbits

(Geeraets) and monkeys (present study), it can be seen that the data are similar.

Until recently, the hazard to the eye consisted primarily of viewing a cw laser over an extended period of time, seconds or even minutes. The problem, it was believed, was one of a steady state temperature equilibrium on the retina of the observer. Basing their evaluation on an assumption that the retina of the human eye will tolerate a 1° C temperature rise for considerable periods of time without sustaining irreversible damage, Jones and Montan[48] calculated that 10^{-6} watts was a safe power level for the retina even when the energy input was considered to be confined to a 10-micron diameter of the retina. Westheimer[36] and most others consider a retinal image size of 10 microns unrealistic because of the inherent aberrations and diffraction problems that exist in the human eye. However, even at this minute image diameter an incident power level of 10^{-6} watts at the cornea can be focused to a power density of no more than 1.33 w/cm^2 on the retina. Therefore, it can be demonstrated that the results of our study (345 w/cm^2 and higher) appear to substantiate the previous authors' contention that 10^{-6} watts at the cornea can be considered a safe level of cw irradiation.

Although it is difficult to compare the effectiveness of the xenon-arc or ruby laser beam and the argon laser beam with regard to their histopathologic damage threshold and clinical usefulness, it has been easily demonstrated that argon radiation is much more highly absorbed by the hemoglobin portion of the retinal structures. An oxygenated blood film has been shown by spectrophotometric studies to absorb seven or eight times more incident energy at the average argon laser wavelengths (5000 Å) than at the ruby laser wavelength (6943 Å). Furthermore, blood agar studies indicate that blood cells are morphologically changed or coagulated with 22 per cent of the energy required to produce a similar coagulation with the xenon-arc beam. Recent studies, to be reported subsequently[37] have shown that the retinal vessels of rabbits and monkeys undergo spasm and occlusion with argon irradiation at a much lower dosage level than with the xenon-arc unit. Brown and Rockwell,[38] Rounds *et al.*,[31] Goldman *et al.*,[39] and others[40,41] have alluded to this unique property of argon laser radiation and have suggested that investigations be conducted to explore the usefulness of this new laser. It would appear that the clinical effectiveness of the xenon-arc photocoagulator in treating vascular lesions is due to the absorption of the shorter wavelengths in the argon

spectral range by these vascular abnormalities. It would be reasonable to assume that the clinical trials with the argon laser, as a pure source of this highly absorbed radiation, will prove to be successful with these vascular disease states.

Precise Focusing Potential

Two important properties of the laser beam are physiologically interesting: the extremely collimated character of the light and its high degree of monochromaticity. The property of extreme collimation implies the possibility of obtaining large energy densities in narrow beams. This particular characteristic can be better discussed by considering the following optical relationship.

The smallest angular displacement, $E_{\min}$, that can actually be resolved by the eye cannot be less than the angular resolution determined by the Fraunhofer diffraction pattern produced by the pupil, regarded as a circular aperture upon which plane wave radiation is incident. Employing the Rayleigh criterion, one finds that $E_{\min} = 2.44\ \lambda/D_E$ where λ is the wavelength of the incident radiation and D_E is the beam diameter or the aperture of the pupil, whichever is smaller.[42] However, in a real eye, the retinal spot is larger than the Fraunhofer spot, and it follows that, if f is the focal length of the eye, the minimal diameter $h_{\min}$ of any retinal image spot is calculated as $h_{\min} = f\ E_{\min}$. By substituting the specific figures for the argon laser, notably a wavelength of 5×10^{-5} cm, a beam diameter (D_E) of 0.22 cm, and an ocular focal length of 17.29 mm, it can easily be established that the minimal retinal image size would approximate 8.4 microns in diameter. This value is several times larger than the theoretical Fraunhofer spot size determined by similar expressions. However, on the basis of the more collimated nature and shorter wavelength of the radiation it is noteworthy that, theoretically, an argon laser can produce a retinal image spot at least seven microns smaller than a comparable ruby laser. The Fraunhofer diffraction relationship cannot be considered with photocoagulation sources such as the xenon-arc high pressure bulb, because the arc radiates energy in a nearly radial fashion. The minimum spot size of the xenon-arc image on the retina has been considered to be between 100 and 150 microns by most investigators, a size close to that produced by the sun.[43] Actual coagulations with the argon laser have been found to be on the order of 20–30 microns in diameter. Using this measured spot size it can be calculated that the

argon laser has the capability of photocoagulating an area (3.14×10^{-6} cm^2) that is approximately 56 times smaller than the minimum coagulation area produced by the xenon-arc system (1.74×10^{-4} cm^2). These values could be particularly significant when the argon laser is used for the precise coagulation of minute portions of the retinal vascular tree.

In addition to exceptional collimation, laser radiation has the feature of being extremely monochromatic. The total argon spectral range covers approximately 700 Å and individual laser transitions can be selected that are less than ten gigacycles in width. Therefore, an argon laser photocoagulator system is not affected by chromatic aberration. A laser emission selected for coagulation can be focused at a particular ocular plane without concern for the effects and individual focus sites of other wavelengths. This monochromaticity of the argon laser beam further enhances the precise focusing potential of this type of radiation.

Pulsing Capability

The extremely high power capabilities of the argon laser permit short exposures or bursts of energy to be used for effective photocoagulation. Although it is expected that most clinical laser applications will employ "painting" techniques at low energy levels, there will be some situations where a minimal amount of energy, transmitted through the ocular medium to the retinal layers, would be desirable. Ham *et al.*,[44] Geeraets *et al.*,[26] Kohtiao *et al.*,[45] and Jacobson *et al.*[46] have shown that the law of reciprocity breaks down with both xenon lamp sources and laser sources of varying pulse duration and intensity. Investigations were undertaken over an extensive range of exposure times from several hundred milliseconds to 30 nanoseconds. It was found that shorter exposures require less total energy for the retinal burns because the short coagulation interval restricts the amount of thermal diffusion. Halving the exposure time does not double the energy required to produce a typically mild lesion. On the contrary, the necessary power density increases by less than the reciprocal of the exposure time, thus defining a radiation dose which decreases with a decrease in exposure time. Therefore, it can be concluded that a mild coagulation of the retina can be produced with less total energy when the system is pulsed at an exposure of ten milliseconds or less. Extremely short pulses of high energy content can be obtained from an argon laser system by electronic shutter devices. Such small retinal energy doses would be advantageous when photocoagulating in the paramacular or

optic disc regions, near vitreoretinal adhesions or fragile vascular lesions, or in the presence of intravitreal blood, strands, or opacities.

High Photon Energy

The process of light emission by an atom accompanies the transition of the atom from a high energy state to a lower energy state. For example, if an atom were in one of the upper laser levels (E_x) and it decayed to the ground state (E_g), it would yield an amount of energy equal to $E_x - E_g$. This energy would be given off as light, the quantum of light energy emitted being called a photon. Since $E_x - E_g$ is the energy available from the change in the atomic state, it can be seen that the larger the energy drop, the higher the frequency and the shorter the wavelength of the emitted light energy[47]: $\lambda = hc/(E_x - E_g)$, where c is the velocity of light (3×10^{10} cm/sec.), λ is the wavelength, and h is Planck's constant (6.55×10^{-27} erg-sec.).

Since the magnitude of the quantum of radiation is inversely proportional to the wavelength, the energy of the quantum of violet light of wavelength 400 millimicrons is twice as great as that of a quantum of red light of wavelength 800 mμ. The energy of the quantum of light of wavelength 500 mμ can be calculated by substituting the proper values in the preceding relationship

$$e = hc/\lambda$$
$$e = (6.55 \times 10^{-27}\ \text{erg-sec.})(3 \times 10^{10}\ \text{cm/sec.})/(5 \times 10^{-5}\ \text{cm})$$
$$e = 3.93 \times 10^{-12}\ \text{erg.}$$

If light of 700 mμ were used instead, the value of e would be 2.80×10^{-12} erg. From these equations it can be calculated that the average argon laser emission has 40 per cent more energy per photon than the ruby laser emission. This energy difference can be considered of practical value if a large amount of energy must be transported in a small concentrated beam. The average diameter of the argon laser beam is 2.5 millimeters, and a power of ten watts compressed into that beam area would create a total unfocused power density of 208 w/cm^2. This value represents a power concentration that is approximately 1550 times the solar radiation constant at the surface of the earth (0.134 w/cm^2). Furthermore, the maximum intensity available from a focused laser has been given by Rempel in the equation

$$I_{\max} = 2.60\, P[(f\lambda)^{-2}/a]$$

in which f is the distance from the lens to the second focal plane (i.e.,

nodal point to retina is 17.29 mm), a is the lens or pupillary aperture radius, and P is power.

The intensity of an incoherent source (such as the xenon-arc bulb), of b watts/cm^2 at the surface is

$$I = b\,a^2/f^2.$$

By combining the last two equations, the ratio F of laser beam intensity at total power P to incoherent light intensity at the focal point is

$$F = 2.60\,P/(b\,\lambda^2).$$

Thus, it can be seen that 5 mw generated by a weak continuous-wave (cw) laser will provide at least 10^5 times greater focused intensity than the most intense incoherent source (250 w/cm^2). These extremely high energies make light energy available in concentrations that conceivably could have a beneficial effect on certain intraocular malignant tumors. Furthermore, photon microsurgery and gross surgical procedures are possible and practical with the energies developed by a powerful argon laser.

CONCLUSIONS

The argon ion laser produces a coherent, monochromatic blue-green beam of intense light energy that has the following unique features of ophthalmologic importance:

1. Argon laser radiation is 4.5 times more effectively absorbed by hemoglobin and vascular structures than xenon-arc radiation.
2. Argon laser energy can be absorbed even more effectively in vascular lesions by the intravenous addition of sodium fluorescein.
3. The TEM_{00} argon beam can be focused to a theoretical spot size at least 40 per cent smaller than any other existing form of light energy.
4. The argon laser can deliver more cw power through the ocular medium and produce a greater cw power density at the retina than any other light source.
5. This blue-green beam has greater inherent energy per photon than any laser source considered for photocoagulation therapy.
6. The argon laser produces radiation that is more highly absorbed per incident photon at the pigment epithelium than any existing photocoagulation system.
7. The argon laser produces radiation that is more highly collimated and directional than any other photocoagulation beam.

8. Argon radiation appears to be absorbed selectively at the nuclear layers, the outer segments of the rods and cones, and the pigment epithelium.

9. The argon laser beam has been adapted optically to several photocoagulation delivery systems for the effective treatment of various ocular and extraocular lesions.

10. An argon laser photocoagulation system has the capability of being pulsed at a predetermined exposure or operated continuously under manual control of the surgeon.

11. The argon laser produces radiation that is seven to eight times more effectively absorbed by hemoglobin than ruby laser radiation.

12. The histopathologic effect of argon radiation on chorioretinal tissue is produced by the absorption of light energy and conversion to heat energy in both the pigment epithelium and the nuclear-receptor layers.

13. Argon radiation creates no detectable adverse effects, other than thermal, on the ocular tissues, plasma proteins, or blood constituents. Nonlinear and acoustic effects have not been demonstrated during these investigations.

SUMMARY

A powerful continuous-wave argon ion laser has been constructed and adapted for ophthalmic use. Optical delivery systems have been devised for the photocoagulation of anterior segment, intraocular, and surface vascular abnormalities. *In vitro* blood studies and qualitative histopathologic investigations were performed in order to delimit the ocular effects of argon radiation. Quantitative threshold damage levels for retinal tissue were determined, and the importance of these studies with reference to future clinical investigations was discussed.

ACKNOWLEDGMENTS

The entire project to develop an argon laser for ophthalmic use was supported by the John A. Hartford Foundation. The concern of the Hartford Foundation was exceptional, and their assistance and understanding contributed immensely to the success of the investigation. The author gratefully acknowledges the assistance rendered by Edward F. Labuda, Ph.D. and August M. Johnson in the physical and engineering applications of the argon laser. Furthermore, the project would have been much more restricted without the interest and technical

knowledge of Eugene I. Gordon and his staff at the Bell Telephone Laboratories in Murray Hill, New Jersey.

The articulated-arm delivery device was machined and assembled at the Bell Telephone Laboratories in Murray Hill, New Jersey. Members of the staff who aided in development of the system are D. R. Herriott, E. I. Gordon, D. A. S. Hale, W. Gronros, and E. F. Labuda.

Considerable gratitude must be expressed to Gordon R. Kelly, M.D., who provided many technical suggestions, critical analyses, and much applied labor during the project. Mrs. Rochelle Singer was of inestimable value in providing histologic preparations and in the general organization of the studies. Mrs. Barbara Vogel and Mr. Heinz Rosskothen were indispensible in many technical functions during the investigations.

Miss Gloria Spevacek, Miss Nancy Walsh, and Mr. Glen Harahan and the medical illustration department staff at the Bronx Veterans Administration Hospital in New York City must be commended for the excellent drawings and photographs included in this thesis.

REFERENCES

1. Maiman, T. H., Stimulated optical radiation in ruby, Nature, 187:493–4 (Aug.), 1960.
2. Zaret, M. M., G. M. Breinin, H. Schmidt, H. Ripps, T. M. Siegal, and L. R. Solon, Ocular lesions produced by an optical maser (laser), Science, 134: 1525–6 (Nov. 10), 1961.
3. Kapany, N. S., N. A. Peppers, H. C. Zweng, and M. Flocks, Retinal photocoagulation by lasers, Nature, 199:146–9 (July), 1963.
4. Campbell, C. J., M. C. Rittler, and C. J. Koester, The optical maser as a retinal coagulator: an evaluation, Tr. Am. Acad. Ophth., 67:58–67 (Jan.–Feb.), 1963.
5. L'Esperance, F. A., The effect of laser radiation on the retinal vasculature, Arch. Ophth., 74:752–9 (Dec.), 1965.
6. L'Esperance, F. A., Clinical comparison of xenon-arc and laser photocoagulation of retinal lesions, Arch. Ophth., 75:61–7 (Jan.), 1966.
7. Campbell, C. J. *et al.*, Clinical studies in laser photocoagulation, Arch. Ophth., 73:57–65 (July), 1965.
8. Koester, C. J. *et al.*, Design considerations for a laser retina coagulator, unpublished manuscript.
9. Verhoeff, F. H., L. Bell, and C. B. Walker, The pathological effects of radiant energy on the eye, Proc. Am. Acad. Arts & Sc., 51:630–818 (July), 1916.
10. Eccles, J. C., and A. J. Flynn, Experimental photo retinitis, M. J. Australia, 1:339–42, 1944.
11. Cogan, D. G., Lesions of the eye from radiant energy, J.A.M.A., 142:145–51 (Jan. 21), 1950.
12. Friedenwald, J. S. *et al.*, Effects of ultraviolet irradiation on the corneal epithelium, II, exposure to monochromatic radiation, J. Cell & Comp. Physiol., 32:161 (Feb.), 1948.

13. Bessis, M., F. Gires, G. Mayer, and G. Nomarski, Irradiation des organites cellulaires à l'aide d'un laser à rubis, Compt. rend. Acad. sc., 255:1010–12 (July), 1962.
14. Geeraets, W. J., R. C. Williams, G. Chan, W. T. Ham, D. Guerry, III, and F. H. Schmidt, The relative absorption of thermal energy in retina and choroid, Invest. Ophth., 1:340–8 (June), 1962.
15. Amy, R. L., and R. Storb, Selective mitochondrial damage by a ruby laser microbeam: an electron microscopic study, Science, 150:756–7 (Nov. 5), 1965.
16. Minton, J. P., A method to determine laser wavelength absorption capabilities of experimental malignant tumors, Life Sc., 3:1007–10, 1964.
17. Rounds, D. E., R. S. Olson, and F. M. Johnson, The laser as a potential tool for cell research, J. Cell Biol., 27:191, 1965.
18. Rounds, D. E., R. S. Olson, and F. M. Johnson, The effect of the laser on cellular respiration, NEREM Rec., 7:106, 1965.
19. Rose, H. W., *et al.*, Human chorioretinal burns from atomic fireballs, Arch. Ophth., 55:205–10 (Feb.), 1956.
20. Zweng, H. C., M. Flocks, N. S. Kapany, N. Silbertrust, and N. A. Peppers, Experimental laser photocoagulation, Am. J. Ophth., 58:353–62 (Sept.), 1964.
21. Vos, J. J., A theory of retinal burns, Bull. Math. & Biophys., 24:115–28, 1962.
22. Rounds, D. E., E. C. Chamberlain, and T. Okigaki, Laser radiation of tissue cultures, Ann. New York Acad. Sci., 122:713–27, 1965.
23. McGuff, P. E., Surgical applications of laser, Springfield, Illinois, Charles C Thomas, 1966.
24. Wolbarsht, M. L., K. E. Fligsten, and J. R. Hayes, Retina: pathology of neodymium and ruby laser burns, Science, 150:1453–4 (Dec.), 1965.
25. Townes, C. H., Optical masers and their possible application in biology, Biophys. J., 2:325–9, 1962.
26. Geeraets, W. J. *et al.*, Laser versus light coagulator: A funduscopic and histologic study of chorioretinal injury as a function of exposure time, Fed. Proc., 24 (suppl. 14): S-48–61 (Jan.-Feb.), 1965.
27. Sjöstrand, F., in G. Smelser, ed., The Structure of the Eye, New York, Academic Press, 1961.
28. Kuwabara, T., and D. Cogan, Tetrazolium studies on the retina, I, introduction and technique, J. Histochem., 7:329–33 (March 9), 1959.
29. Pearse, A., Localization of oxidative enzymes in rat and chick retina in various physiological conditions, in G. Smelser, ed., Structure of the Eye, New York, Academic Press, 1961.
30. Milne, L., and M. Milne, in Handbook of Physiology, Neurophysiology, Washington, D.C.: Am. Physiol. Soc., 1:621–45, 1959.
31. Rounds, D. E., R. S. Olson, and F. M. Johnson, Wavelength specificity of laser-induced biological damage, Presented at the Electron, Ion, and Laser Beam Technology Symposium: Berkeley, California, May, 1967.
32. Wald, G., P. Brown, and P. Smith, Iodopsin, J. Gen. Physiol., 38:623–79 (Nov. 10), 1954.
33. Rushton, W., and F. Campbell, Measurement of rhodopsin in the living human eye, Nature, 174:1096, 1954.
34. Chapman, D., in The Structure of Lipids by Spectroscopic and X-Ray Techniques, New York, John Wiley 1965, p. 50.
35. Ham, W. T. *et al.*, Optical masers (lasers), Acta Ophth., 76 (suppl.): 60–78, 1963.
36. Westheimer, G., Optical and motor factors in the formation of the retinal image, J. Opt. Soc. Am., 53:86–93 (Jan.), 1963.

37. Kelly, G. R., and F. A. L'Esperance, The effect of argon radiation on the retinal vasculature, Arch. Ophth., to be published.
38. Brown, T. E., and R. J. Rockwell, Jr., The argon laser: its effects in vascular and neural tissue, Read at the IEEE 9th Annual Symposium on Electron, Ion, and Laser Beam Technology, Berkeley, California (May 11), 1967.
39. Goldman, L. *et al.*, The biomedical aspects of lasers, J.A.M.A., 188:302–6 (April 20), 1964.
40. Litwin, M. S., Epilogue—a summing up, Fed. Proc., 24:5175–7 (Jan.-Feb.), 1965.
41. Bush, I. M., W. F. Whitmore, Jr., and P. H. Lieberman, Experimental surgical applications of the laser, Read at the annual meeting of the A. Adv. M. Instrumentation, Boston, Mass., July 27, 1966.
42. Solon, L. R. *et al.*, Physiological implications of laser beams, Science, 134: 1506–8 (Nov. 10), 1961.
43. Meyer-Schwickerath, G., Light Coagulation, St. Louis, Mosby, 1960.
44. Ham, W. T., H. Wiesinger, F. H. Schmidt, R. C. Williams, R. S. Ruffin, M. C. Schaffer, and D. Guerry, Flash burns in the rabbit retina as a means of evaluating the retinal hazard from nuclear weapons, Am. J. Ophth., 46: 700–23 (Nov.), 1958.
45. Kohtiao, A., J. Newton, H. Schwell, and I. Resnick, Hazards and physiological effects of laser radiation, Ann. New York Acad. Sc., 122:777, 1965.
46. Jacobson, J. H., B. Cooper, and H. W. Najac, Effects of thermal energy on retinal function, Tech. Doc. Rep. No. AMRL-TDR-62-96, USAF Project No. 6301, Task No. 630103 (March), 1962.
47. Jenkins, F. A., and H. E. White, Fundamentals of Optics, 3rd ed., McGraw-Hill, 1957.